공학박사학위논문

Electron Beam Induced Ductile Enhancement and Large Strain Plasticity of Cu Thin Films

전자빔 조사를 통한 구리 박막의 연성 향상과 극 인장변형에서의 구리 소성 거동 연구

2017년 8월

서울대학교 대학원

재료공학부

이 소 연

전자빔 조사를 통한 구리 박막의 연성 향상과 극 인장변형에서의 구리 소성 거동 연구

ELECTRON BEAM INDUCED DUCTILE ENHANCEMENT AND LARGE STRAIN PLASTICITY OF CU THIN FILMS

지도교수: 주 영 창

이 논문을 공학박사 학위논문으로 제출함

2017년 8월

서울대학교 대학원

재료공학부

이 소 연

이 소 연의 박사학위 논문을 인준함

2017년 7월

위 원 장	오 규 환	(인)
부 위 원 장	주 영 창	(인)
위 원	황 농 문	(인)
위 원	한 흥 남	(인)
위 원	최 인 석	(인)

ABSTRACT

Electron Beam Induced Ductile Enhancement and Large Strain Plasticity of Cu Thin Films

So-Yeon Lee
Department of Materials Science and Engineering
The Graduate School
Seoul National University

As flexible devices become a new paradigm of electronic devices in the future, researches for improving the reliability of flexible devices are attracting attention. Since the reliability of the flexible device is closely related to the reliability of the metal thin film underlying the electrical characteristics of the device, the reliability improvement of the metal thin film leads to the improvement of the reliability of the flexible device. Unlike metal thin films deposited on conventional rigid and unmodified substrates, metal thin films deposited on flexible devices are exposed to continuous mechanical deformation. The destruction of the metal thin film due to the mechanical deformation soon leads to the deterioration of the electrical properties and causes the destruction of the device. Therefore, it is essential to understand the development of metal thin films with excellent mechanical reliability and the deformation mechanism to make them possible.

The rapid destruction of the metal film is caused both in material and structural aspects. In the material aspect, plastic deformation is difficult because the displacement of the dislocations within the crystal is limited due to the reduction of the grain size due

to the thinning of the material. In addition, the number of dislocation sources is also small, and it is impossible to generate dislocations continuously for plastic deformation. Therefore, a material having a small grain size does not undergo plastic deformation and undergoes a straight failure after elastic deformation. On the structural level, on the other hand, the dislocations in the material easily escape to the surface therefore plastic deformation is inhibited, as well as stress localization at the curvatures and defects of the surface causes rapid destruction of material. The maximization of the surface effect can be solved to some extent by a method of increasing the thickness of the structure by depositing the thin film on the substrate. In this case, the fracture mechanism of the metal film is affected by the difference in the mechanical properties of the two materials, since it must move with a flexible substrate having a lower modulus and a higher elastic limit strain than the metal film. Particularly, the difference in mechanical properties causes delamination of the metal thin film during tensile deformation. Since the delaminated metal thin film follows the deformation in the state of free-standing film, delamination causes destruction of the metal thin film.

Therefore, in order to design a metal thin film having excellent mechanical reliability, it is necessary to design a structure that suppresses delamination. When the metal thin film is uniformly deformed along the flexible substrate without separation, the plastic deformation is evenly caused, and deformation can be performed without destruction. In addition, when such a structure is made, the potential must be steadily supplied to the inside of the metal so that the plastic deformation can be made steadily. That is, it is necessary to design a microstructure capable of continuously applying dislocations to the inside. For this purpose, a comprehensive understanding of how the microstructure of the thin film changes during tensile deformation should be given priority. However, since the grains existing in the thin film are smaller than the resolution of the electron

backscattering diffraction (EBSD), which is a commonly used microstructure analysis instrument, there is a problem that it is difficult to analyze the microstructure with the existing EBSD.

In this study, the design of the structural layer to improve the reliability of the copper thin film, which is a typical conductor used in electronic devices, was conducted through a new method called electron beam irradiation. When the electron beam is irradiated onto the copper thin film, the adhesion between the copper thin film and the flexible substrate is improved, and the peeling of the copper thin film is suppressed. Therefore, the fracture of the thin film due to the peeling was suppressed, so that the surface showed almost no crack even under the tensile strain of 30 %. Improvement of interfacial adhesion of electron beam irradiation was confirmed by nanoscratch test and nanoindentation test, and it was confirmed that the flexible substrate deformed by electron beam causes improvement of adhesion. Based on that the excellent mechanical properties lead the excellent electrical properties, it is possible to fabricate a phosphorescent organic light-emitting diode (OLED) that does not break down in the irradiated area under deformation, and it can be used as a patterning technology for fabricating a flexible device and a responsive device in the future

The microstructure deformation mechanism of copper thin films was also investigated by mechanical deformation of copper thin films. For microstructure analysis of grains of size near 100 nm, microstructure analysis was carried out using ASTAR™, a microstructure analysis technique based on a transmission electron microscope instead of the conventional EBSD. As a result, it was confirmed that the high density twin boundary existing inside the copper thin film helps to relieve the stress and strain energy inside the material through the microstructure change rather than the crack. The twin boundaries not only cause coarsening of grains in the process of

propagation between grains, but also cause refinement of grains by making twin boundary - dislocation structure through interaction with dislocations generated at twin boundaries. Through the microstructural change, the copper thin film irradiated with the electron beam could continue the plastic deformation continuously without breaking even under the high tensile strain.

In this study, it is shown that the microstructures can be improved by plastic deformation if the steady dislocation supply and strain localization are solved even in materials with fine microstructure, which are known to be brittle. Based on the work, the design criteria of metal thin film materials to improve the performance and reliability of flexible devices are presented.

Keywords: Metal, mechanical behavior, deformation mechanism, flexible device, Copper thin film, interfacial adhesion, electron beam irradiation, microstructural analysis

***Student Number*:** 2011-20657

Table of Contents

LIST OF TABLES

LIST OF FIGURES

Figure 4.11 (a) Hardness of both untreated and treated sample by nanoindentation. (b) Difference of hardness before and after irradiation. Cross section image of interface of (c) electron beam untreated and (d) e- beam treated sample by TEM. (e) Critical normal force, normal force at the first delamination of Cu film from PI, is measured from both electron beam untreated and electron beam treated Cu. Relative work of adhesion (L_{crit}/L_{crit0}, where L_{crit0} is the work of adhesion of the electron beam untreated). Work of adhesion could be calculated by using critical normal force. SEM image of e- beam untreated (f) and e beam- treated (g) Cu thin film after scratch test. Scale bars, 100 nm (c, d); 50 μm (f, g)

Figure 4.12 (a) Cu pad on polyimide substrate without any electron beam irradiation and (orange square) Cu pad on polyimide substrate which is irradiated by electron beam prior to the deposition of copper thin film (yellow square). (b) and (c) are the magnification of copper in orange and yellow square of (a), respectively. Scale bars, 100 μm (a); 1 μm (b)

Figure 4.13 XPS result of C and O spectrum of electron beam untreated polyimide and electron beam treated polyimide. After electron beam irradiation, amount of C=O bonding decreased and C-O bonding increased.

Figure 4.14 (a) Schmatic of in-situ sheet resistivity measurement and (b) FE-SEM images of the electrical resistivity measurement of e-beam treated films at a tensile strain of 30 % (E-beam irradiation condition: acceleration voltage of 25 kV, probe current of 10 nA, and irradiation time of 10 min). (c) Electrical resistivity of the as-deposited and strained (ε=30 %) Cu films with and without e-beam irradiation. Resistivity measurement of the strained Cu films was conducted using the 4 point probe method while maintaining the final strain using a tensile jig.

Figure 4.15 (a) OLED preparation: Cu 100 nm film for bottom electrode deposited on PI, then Cu is patterned with smile using FIB scanning. After patterning, active materials and top electrode are deposited on Cu. (b) Structure of OLED. Photographs of the stretchable OLED at 8 V with strain values of 0 % (c), 3 % (d), 3.5 % (e), 4 % (f), and 4.5 % (g). Scale bar, 500 μm.

Figure 5.1 ASTAR™ results of Cu thin films on Polyimide substrate before and after tensile deformation. Invert pole figures of (a) 0 % strain, (b) 6 % strain, (c) 10 % strain and (d) 20 % strain and image quality map with misorientation of (f) 0% strain, (g) 6 % strain, (h) 10 % strain and (i) 20 % strain, respectively. (j) Average grain size and (k) distribution of misorientation varying tensile strain Scale bars, 300 nm (a-i)

CHAPTER 1

Introduction

1.1. Background

Flexible devices are based on soft substrate which could be able to bend, fold, and twist, contrary to conventional rigid and undeformable substrate. Today, flexible device is the ultimate goal of electrical device which have led to modern era. Especially, the requirements of wearable devices, which can only be continuous deformation, and attachable devices, which could be easily controlled and communicated over long distances, have gradually increased over the time, therefore flexible engineering has become a key technology for manufacturing these devices. Fabrication of flexible device has begun with the production of device on curved substrate, has reached to manufacture flexible / bendable displays and sensors, and now aims to manufacture devices that can withstand severe deformation such as folding, stretching and twisting. The flow of flexible device manufacturing technology is summarized in Figure 1.1. Accordingly, studies have been eagerly made on a technique for designing a flexible device that does

not lose the mechanical / electrical properties under continuous and severe deformation, and a failure mechanism of flexible device for solving the reliability problem.

Conventional rigid electrical devices consist of silicon substrate, metal electrode and interconnects, and transistors based on metal oxide. That is, it is composed of the materials having similar mechanical properties. Therefore, only the failure due to the inherent characteristics of the material should be considered when the device is deformed. However, because it is based on polymer substrate which has quite different mechanical properties compared to metal and ceramic as shown in Figure 1.2, the failure mechanism is more complex in case of flexible devices. Failure of flexible device is based on delamination because not only the ductility of the material is insufficient, but also the inconsistent mechanical behaviors of the materials due to different mechanical properties of the materials during deformation.

To solve this problem, the reliability design study of flexible devices is proceeding in the direction of designing materials with more flexible - close to the mechanical properties of the substrate - and in designing the mechanical deformation stability of two materials showing different behaviors. In this study, we focus on the reliability design problem of the flexible device for the copper thin film, which is the core material of the electronic device.

The texture and microstructure of copper are closely related to each other. In the case of conventional bulk and micro - sized films, active research on microstructure has led to the development of mechanical properties of copper. The researchers increased the strength by reducing the grain size of copper[1-5], and also increased ductility by incorporating defects such as precipitation and alloying[6-8], which could cause strain hardening inside. Unlike bulk copper, which has elongated to tens of percent based on

such microstructure design technology, copper thin films used in electronic devices suffer from cracks even when tensile strain of only a few percent is applied[9-12].

However, due to limitations of analytical techniques, fundamental understanding of the mechanism of deformation and crack formation has not been achieved. Instead, the reason for the rapid breakdown of copper films compared to bulk is explained by limited methods such as non-comprehensive local analysis or phenomenological macro analysis based on various assumptions and simulations. First, the copper film is composed of nanocrtystlline and ultra-fine grain, which is known to be brittle than bulk Cu in the case of nc-ufg Cu. This is because as the size of the grain decreases, the amount of defects existing in the grain becomes smaller, so that the dislocation source becomes smaller and the space (grain size) capable of accommodating the dislocation becomes smaller. Second, since the thin film is thinner than the bulk, the volume that can accommodate the instability generated in the defect inside the copper is small, so that the concentrated stress in the defect easily exceeds the yield stress of the material.

However, there are still many questions about how copper thin films are deformed and destroyed by the existence of twin, grain size, and grain boundary characteristics. In addition, due to limitations in understanding these fundamental deformation characteristics, it is difficult to propose a solution to overcome the mechanical limitations of copper thin films used in flexible devices.

Figure 1.1 Trend of electronic device development. Starting with a wafer-based rigid element, a flexible element based on a flexible substrate is under development and ultimately aims to develop a wearable device.

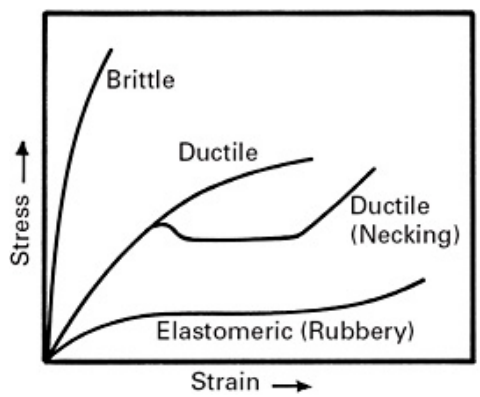

Figure 1.2 Mechanical properties of different materials. Brittle and ductile behaviors are shown from metal, and elastomeric behaviors are shown from polymer materials. Difference of mechanical properties of two materials causes reliability issue on flexible device.

1.2. Motivations

1.2.1. Technical driving force

In order to solve the reliability problem of copper thin films in flexible devices directly related to the performance of devices, in other words, to increase the ductility of copper thin films, the following studies are carried out at the view of microstructure of the material and at the view of the system.

In the microstructural view of materials, researches have been actively carried out to induce work hardening by implanting nanotwin in ultra-fine grain to improve ductility of copper[13-17]. Nanotwin acts as a defect in the grain and serves as a source to generate dislocations. It also changes itself through twinning / detwinning and affects the microstructure change of copper due to stress. However, the results of this study are mainly in the bulk dimension, and the relationship between the microstructure and the ductility enhancement in the thin film is insufficient. This discussion will be discussed in more detail in the 1.2.2 described below.

On the systemic view, the adhesive force between the substrate and the thin film is improved so that 1) the peeling of the substrate is suppressed so as not to show the behavior of the free standing film having high brittleness, 2) the necking is suppressed. This study first describes the process of peeling a metal thin film deposited on a flexible substrate through FEM simulations and describes the effect of the adhesion at the interface and the stiffness difference between the substrate and the metal on the detachment of the metal thin film during tensile deformation[18-20]. The above results show that the adhesion is excellent and the stiffness difference between the two materials is controlled by controlling the thickness and the elastic modulus of the material, the

delamination of the substrate is suppressed and the crack generation is suppressed accordingly. Based on this, studies have been made on crack generation according to the thickness of the metal thin film and crack suppression through the improvement of the adhesion strength, particularly, due to the practical problem that the thickness of the thin film is limited by application. However, the strain value of formation of cracks which are reported in the above study still does not exceed 10%. In the case of wearable devices, which are considered to be the ultimate goal of flexible devices, thin film-substrate composites are required that do not break even at higher strains, as they must withstand strains of up to 20%. In addition, most reliability studies have been reported on the basis of resistance variation due to tensile strain rather than direct crack observation. However, even if the same metal film is deposited on a flexible substrate alone, there is a difference between the deposition of only one layer and the change of the device on the metal film. That is, the resistance change value of the copper thin film does not represent the resistance change value when it is made into the device. The device can react more critically. Therefore, there is a need for a technique for designing a copper thin film so as to have high reliability even when a device is actually placed on the copper thin film.

Other approaches include designing the shape of the electrode as a horseshoe or mesh structure, or depositing a copper film on a pre-tensioned substrate to form a thin film-substrate composite[22,23] (Figure 1.4). One common feature of these techniques is that the strain across the copper film is dispersed circumventively through displacement changes. However, these studies limit the directivity of the device as the patterning process is complicated and the area occupied by the wiring in the device increases. Therefore, it is economically incompatible to introduce it into mass production from the lab scale. In addition, since the strain is solved in a circumferential manner, not controlled by the material itself, when a strain larger than strain which can be solved by displacement is

applied, copper thin film in these work goes to fail due to the intrinsic material property. Therefore, there is a need for a new method to improve the ductility of thin metal film on flexible substrate by simple and inexpensive process which is used in the fabrication of existing electronic devices.

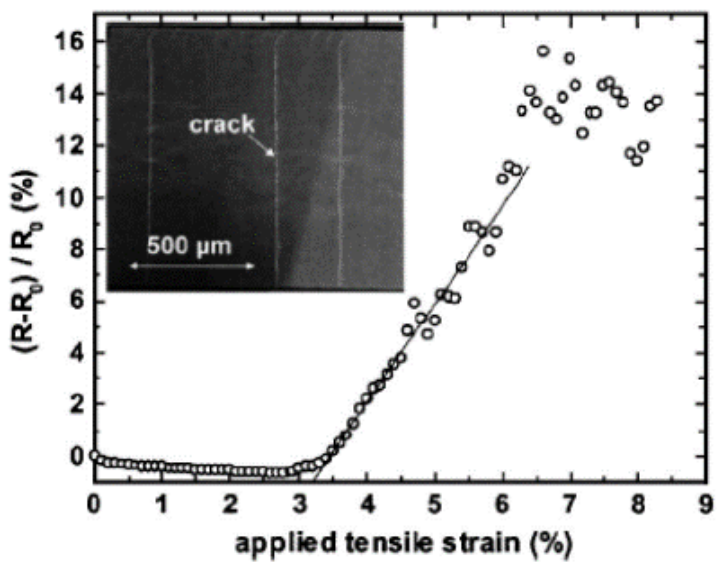

Figure 1.3 Failure of electrical properties of metal due to generation of cracks during elongation.[21]

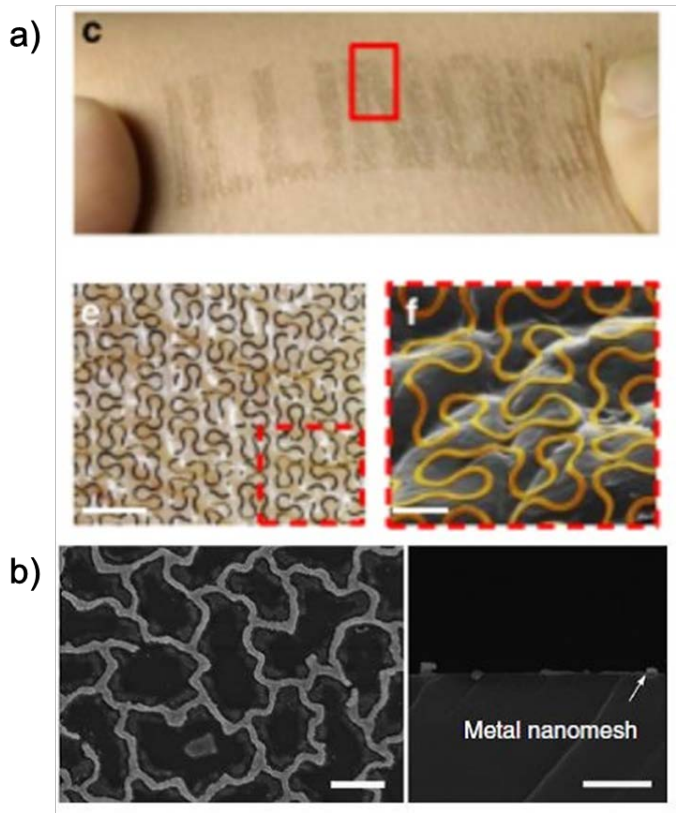

Figure 1.4 (a) Horseshoe[22] and (b) mesh time[23] of electrodes for flexible devices. Both electrodes are based on the relieve mechanism which transfers strain energy to the displacement of materials rather than elongation of materials.

1.2.2. Scientific driving force

As described above, the mechanical properties of the material are closely related to the microstructure of the material. Therefore, understanding of the microstructural changes of materials due to deformation is essential for the design of materials and the development of materials suitable for the application.

In conventional bulk materials, microstructure analysis was done via electron backscattered diffraction[24,25] (EBSD). EBSD is a technique for observing the microstructure of a metal using a scanning electron microscope. It is a technique for analyzing the microstructure of a material based on information such as the angle and intensity of the electron beam scattered when the electron beam is irradiated on the sample. Unlike x-ray diffraction (XRD), which can interpret changes in the behavior of specific orientations, EBSD has the advantage of intuitively and universally identifying the microstructure of the material as seen through a scanning microscope. Due to such convenience, the relationship between the microstructure and the mechanical properties of metals using EBSD has been actively researched. However, since the thin film has a microstructure smaller than the resolution of the conventional EBSD, it is impossible to analyze the microstructure through the EBSD. In general, the resolution of EBSD is about 300 nm. The thin film usually has a grain size of about the thickness of the thin film, further, when the defect exists inside the crystal, the size of the defect is much smaller. Hence it is hard to confirm exactly what kind of microstructure change the deformation behavior caused. In addition, the metal thin film used as the conductive material of the flexible substrate has a shape that is deposited on the polymer substrate, but the polymer substrate is not conductive. Therefore, when observing the microstructure of a metal deposited on a polymer substrate by using an electron beam,

an electron beam is charged on the substrate and image scanning is not possible. Additionally, since the substrate itself may be changed by an electron beam, in the case of thin films, microstructure analysis was more difficult.

For this reason, research on the relationship between the mechanical behavior of metal thin films and the microstructure inside the metal is almost impossible. However, recently, a new analytical instrument has been devised and the microstructure of the thin film is observed started. In addition, attempts have been made to minimize the effect of polymer substrates on electron beams by reducing the thickness of polymer substrates through various methods. Therefore, based on the above method, it is necessary to study the microstructure of the copper thin film based on the new analytical method of analyzing the microstructure with smaller resolution by separating the PI from the metal thin film.

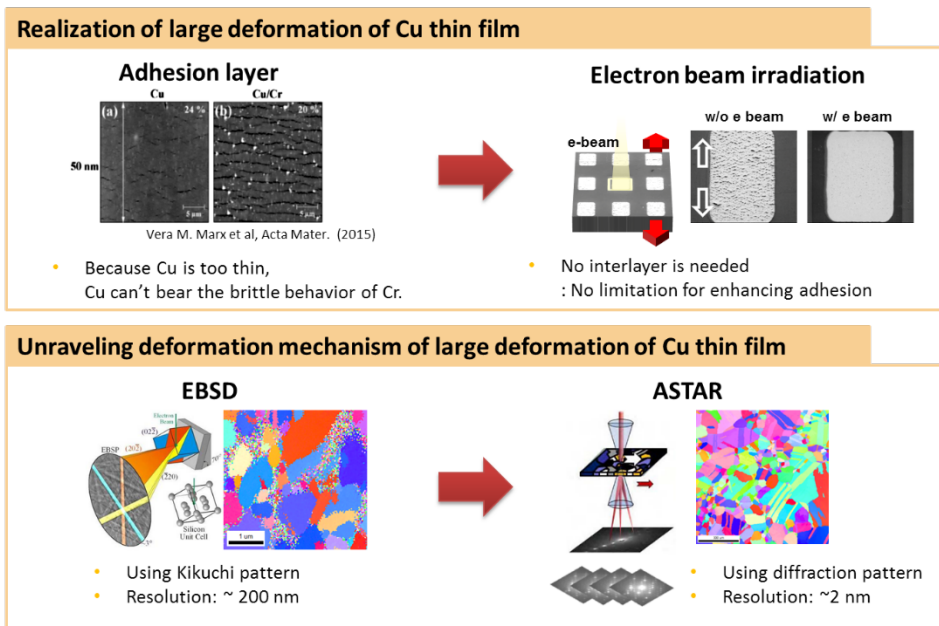

Figure 1.5 Strategy of this study based on electron beam irradiation and TEM-based EBSD analysis.

1.3. The goal of and outline of this research

In this study, we fabricated a copper thin film - polyimide substrate composite which improved the adhesion through electron beam irradiation and hardly cracked even at a strain of 30%. Based on electron beam technique, we could develop strain-responsive OLED which was driven only with patterned area when tensile strain was applied. The details of this work will be introduced in Chapter 4 after discussing basic theoretical backgrounds in Chapter 2 and experimental procedure in Chapter 3. After removing the polyimide substrate through grounding, we investigated how the microstructure of the copper film changes with tensile strain using TEM-based EBSD (ASTAR^{TM}) with a resolution of several nanometers. As a result, copper thin films containing high density nanotwin have been found to undergo grain coarsening and refinement as the tensile deformation progresses, thereby eliminating the strain on the system without cracking. The details of deformation mechanism of Cu thin will be introduced in Chapter 5, and thesis is finished with conclusion in Chapter 6.

CHAPTER 2

Theoretical background

2.1. Deformation mechanism according to microstructure of Cu

The deformation mechanism of the metal material is closely related to the microstructure of the metal. This is because the driving mechanism that moves the atoms in the material depends on the microstructure. In particular, the grain size is the most important microstructure factor affecting the strain mechanism of the material because the size of the grains affects the stress applied inside the grains. Therefore, in this chapter, the microstructure will be classified into grains of micron scale and grains of nano scale according to the grain size, and then the microstructure deformation mechanism will be explained. We will also explain the twin-induced deformation mechanism of microstructure found in materials with low staking fault energy such as copper.

2.1.1. Coarse grain Cu

A coarse grain (CG) is a grain that is usually about the size of a micron. The

deformation mechanism of such a coarse grain is mainly based on the generation and movement of dislocation, and occasionally includes deformation twin. Dislocation is a defect in the material that facilitates the movement of atoms even at stresses below the theoretical stress that are required when the atoms move away from each other directly. Dislocation plays a key role in the deformation mechanism of the metal due to external forces. Therefore, how easily the dislocations in the material exist and how well it can move determines the ease of deformation of the material. Dislocations are generated and moved upon by the source of various types, the interaction with other dislocations, and the interaction with other microstructural elements such as solute atoms, precipitate, grain boundary, and phase boundary[26, 27]. The amount of dislocations generated through this process decreases as the size of the grain decreases, because the smaller the size of the grain, the lower the probability that the source capable of generating dislocations decreases. In addition, because the dislocation is basically a mismatch of the atomic arrangement, a stress field is formed around the dislocation. Thus, as the dislocations approach the distance, i.e., the dislocation density in the grain increases, the dislocation densities of the grains play a large role in determining the movement of the dislocations since the interaction of the stress fields has a great influence on moving the dislocations. In addition, when the size of the grain is small, the space where the dislocations can move becomes small, so that the interference between the dislocations becomes severe, and the dislocation movement becomes difficult[28]. Based on this phenomenon, the mechanical properties of the material according to the grain size are explained in the following relation in the coarse grain, very well known as Hall-Petch relationship (Figure 2.1 and Figure 2.2).

$$\sigma_y = \sigma_0 + kD^{\alpha}$$

Here σ_y is the yield stress, σ_0 is the frictional stress required to move dislocation, k is the H-P slope, and D is the grain size. In the case of coarse grain, α has a value of 0.5. As the grain size decreases, the increase in σ_y is usually accompanied by a decrease in the ductility. As the magnitude of the stress on the material increases, the stress value concentrated in the local part increases the probability of having enough value to break the bond to be.

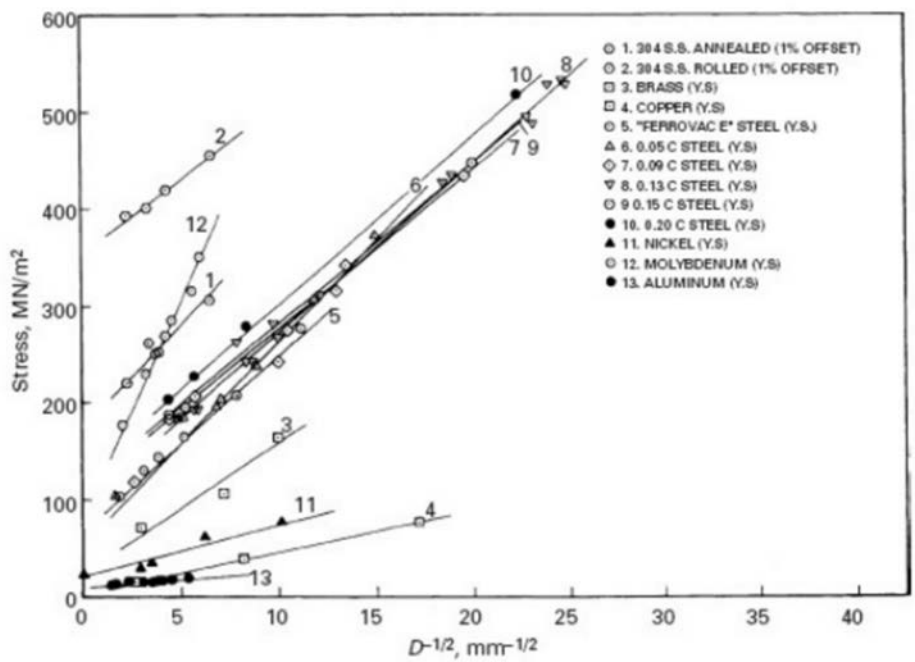

Figure 2.1 The relationship between strength and inverse of square root of grain size, also known as Hall-Petch relationship.

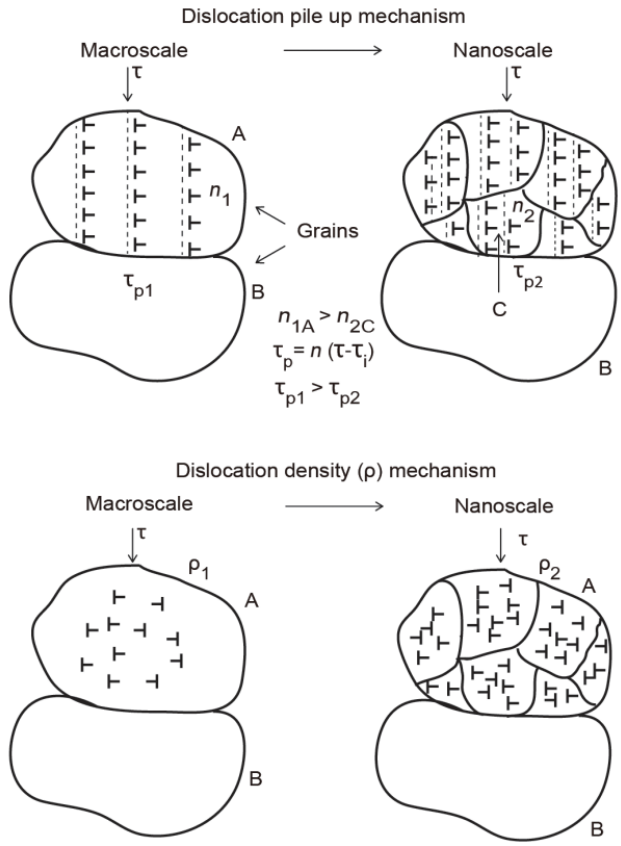

Figure 2.2 Schematics of the mechanism of Hall-Petch relationship. Because of small grain size, amount of dislocation in the grain is fewer than large grain but the dislocation density is higher. Therefore, larger stress is required to move dislocation over the grain boundary due to fewer dislocations for pileup, and to generate dislocations due to higher dislocation density[28].

2.1.2. Ultrafine grain and nanocrystalline Cu

Ultrafine grain (UFG) is defined as submicron sized grain and nanocrystalline is defined as grained tens of nanometers. As shown in Figure 2.3, the deformation mechanism of the material depends greatly on the size of the microstructure, especially the grain size. When the coarse grain of large size shows the deformation mechanism based on the dislocation, the nanocrystalline shows a deformation mechanism depending on the grain boundary, and in ultra-fine grain, dislocation-mediated mechanism and grain boundary-mediated mechanism occurs competitively[17] (Figure 2.4).

UFG metals have CG-like dislocation based mechanisms, except that dislocation cells with a large number of dislocations are not observed because the number of dislocations relative to coarse grains is small - the number of dislocations source per grain is small. When the grain size is close to that of nanocrystalline, the number of atoms in the body of the grain and the number of atoms corresponding to the grain boundary gradually become similar, increasing the dependence of the deformation mechanism upon the movement of the grain boundary. The k/D trend, which increases in strength as grain boundaries, and therefore grain size, are still similar, varies α or k. Usually, α has a value larger than 0.5 in UFG[29-31].

The deformation mechanism of nanocrystalline (NC) metal is more complicated than UFG. In this nano-sized region, mechanisms based on the movement of grain boundaries predominate over dislocation-based mechanisms. Since the size of crystal grains is very small, dislocation forest cannot be formed due to a small number of dislocation sources in the grains, and space for moving dislocations within the crystal

grains is limited. In addition, as the area of the grain boundaries is wider than that of the grain, the dislocations easily escape to the grain boundaries where atoms are disordered, making it difficult to collect dislocations within the grain. Therefore nanocrystalline deforms based on grain rather than dislocations. Representative examples of deformation mechanisms based on grain boundaries are grain boundary sliding[32], grain rotation[33], and grain boundary migration[34], both of which occur together rather than predominantly dominant[35-39].

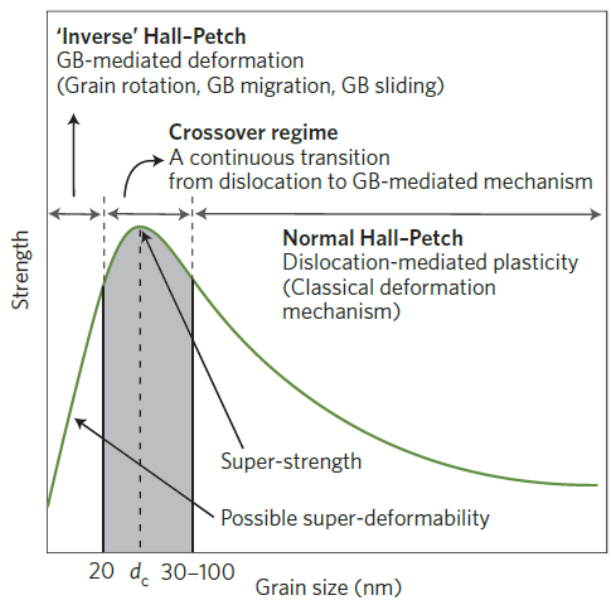

Figure 2.3 Transition of deformation mechanism as grain size reaches to the nanocrystalline from coarse grain[17].

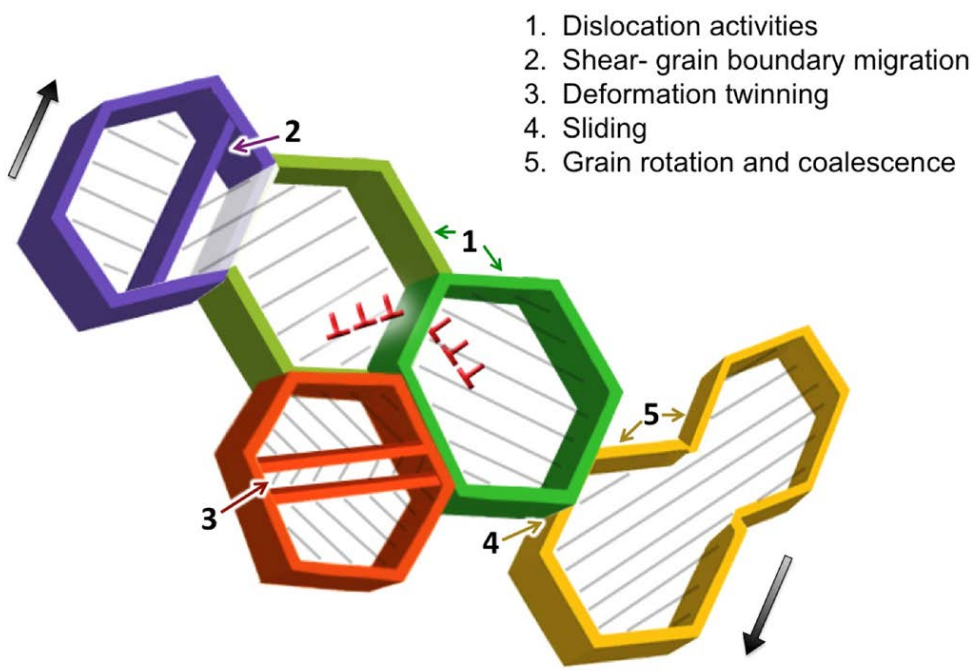

Figure 2.4 Schematic of the grain boundary-mediated deformation mechanisms; grain boundary migration, grain sliding, grain rotation and coalescence.[40]

2.1.3. Nanotwin Cu

Besides the deformation mechanism based on the dislocation and grain boundary described above, there is another deformation mechanism based on a stacking fault. Unlike the point or line-level potential, the stacking fault is a method of eliminating the mismatch of material in the plane dimension. In case of metals with low stacking fault energy that are easy to generate staking faults, stacking faults, i.e., twin-based deformation mechanisms are shown instead of mechanisms based on the slip of perfect dislocations. When deformation occurs under high strain rate, or at low temperature, twin-mediated deformation mechanism can be occur in metals with high stacking fault energy[41-48].

Twin improves both the strength and ductility of the material[13,49-53] . If the grain size is small, the internal defects are also reduced, so that the dislocations within the grain cannot be fixed and amplified, and they escape through the grain boundary or the surface. However, if there is a twin inside the crystal, the dislocations cannot move due to the twin boundaries, so that the dislocation can be pinned into the crystal grains, so that the material can have greater strength[54-57]. On the other hand, the twin also serves as a dislocation source and a moving path for dislocation[13, 58, 59].

There are two main ways of generating dislocations in a twin: one is the generation of dislocations with a slip plane perpendicular to the twin plane from the step inside the twin, and the other is the interaction between the twin and grain boundaries and generate dislocation with a slip plane parallel to the twin plane near the twin-grain boundary junction[60, 61]. The dislocation from those mechanisms move along its slip plane or along the twin planes hence twin boundary induces strain hardening that is not possible in ultra-fine grain and nanocrystalline (Figure 2.5). That is, twinned metal can have high

ductility as well as high strength because it makes continuous generation of dislocations and movement of dislocations easy. Because twin can steadily apply dislocations inside the ultra-fine grain and nanocrystalline which has no dislocation source inside can have twin-based plastic deformation.

In addition, the twin relieves the strain energy applied in the grain by modifying itself[62-65]. As shown in Figure 2.6, the twin generated inside the grain may propagate or disappear by the movement of the twinning partial as deformation occurs. Or twins are created inside the grain through deformation as deformation twin. Through such twinning / detwinning, the material can steadily undergo plastic deformation, resulting in increased ductility of the material.

Compared to other microstructure control processes, nanotwin has the advantage of improving strength, ductility and electrical conductivity[13] (Figure 2.7). Copper is one of the most actively studied metals characterized by nanotwin formation due to low stacking fault energy. Starting with the report of mechanical and electrical properties in science in 2004 by Lu, some hundreds of studies have been published to date. Based on such active research, the properties of copper have resulted in more than 4 times the strength and more than 5 times the elongation improvement. By embedding twin inside of the grain. This active twin-copper study has been a great help in understanding the characteristics of the twin and has helped to understand the behavior of twin in other materials.

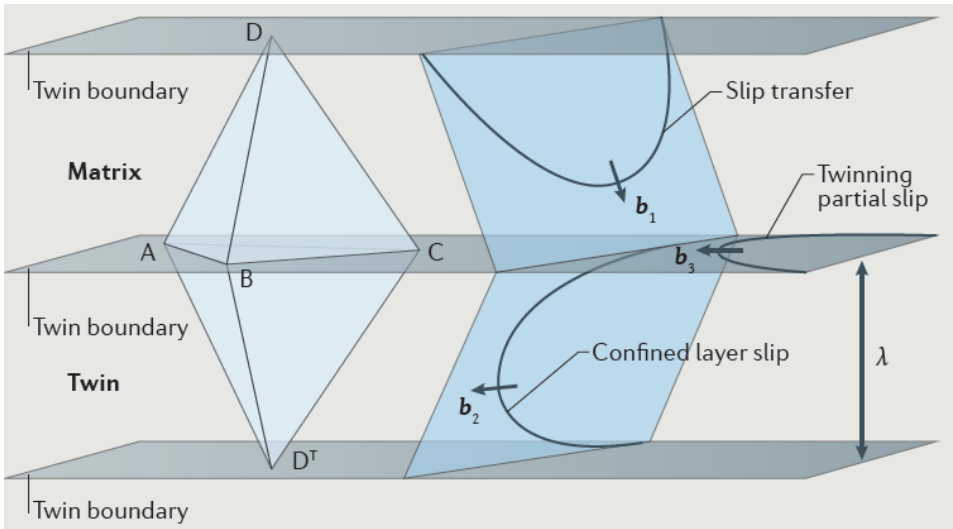

Figure 2.5 Schematic of the relationship between twin boundary and dislocation; slip transfer mode (Hard mode I), confined-layer slip mode (Hard mode II), twinning partial slip mode (soft mode)[60].

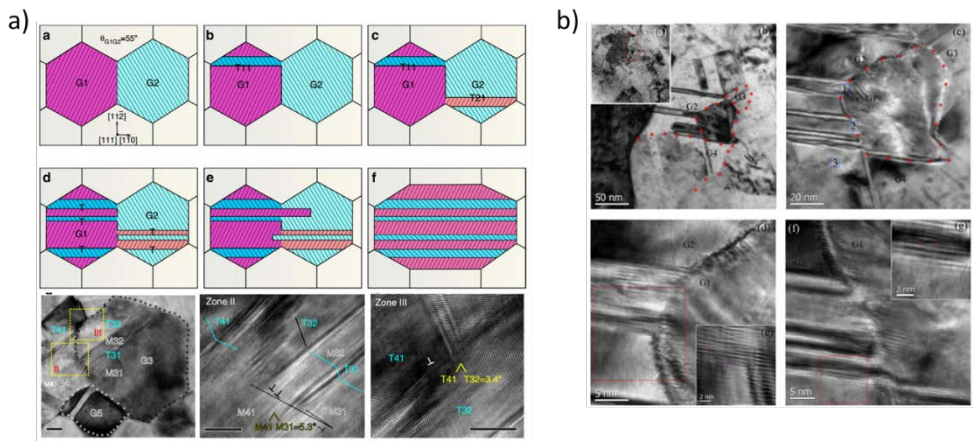

Figure 2.6 Interaction between nanotwin and grain boundary in (a) Au[62] and b) Ni[63]. When twins reach to the grain boundary, twin dissipates grain boundary.

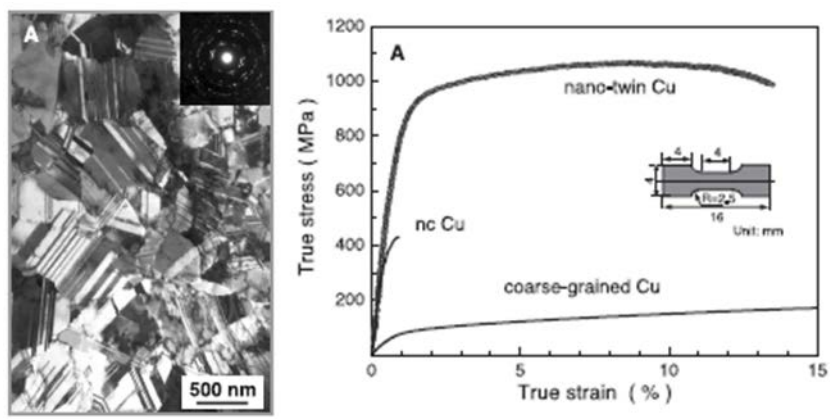

Figure 2.7 Microstructure and its stress-strain curve of nanotwinned Cu[13].

2.2. Ductility of thin metal films on polymer substrates

2.2.1. Limited elongation in freestanding thin metal films

The smaller the material size, the more the intensity is not the only story of the microstructure. On a structural level, thin films have higher strength than bulk materials (Figure 2.8a). The characteristic of such a structural material is that it has a very fine microstructure in the direction of thickness, and the increase in the strength of the material is also based on the Hall-petch effect to a certain extent. But the above is not all. The following are system considerations.

First, the thin film consists of a very small number of grains, sometimes one grain, in the thickness direction, which means that the influence of the free surface is larger than the grain boundary or defects in grain. The free surface promotes the escape of dislocations, so the amount of dislocations that escape through the surface is much greater than the amount of dislocations generated by deformation within the grain. This exhaustion hardening, or in other words, the phenomenon referred to as dislocation starvation, prevents the accumulation of dislocations within the grains and thus has a significant effect on the mechanical properties of the material.[66-69] As well as the problem of small grain size, thin film materials have a smaller volume of system than bulk materials, so the amount of dislocation sources is small, and the dislocation source is also easily removed through the free surface. Because of this, the dislocation source is hard to activate.

The roughness of the surface is also one of the problems that arise as the surface effect in thin film deformation prevails[70,71]. Unlike an ideal surface, the surface of the actual material is not smooth and there is roughness on the atomic scale. This may be due to

an inhomogeneous deposition process and may be due to defects present on the free surface like grain groove. This roughness acts as a stress concentration spot, resulting a local stress concentration, which causes deformation and fracture of the material with only a few percent deformation.

For the above reasons, the thin film usually has a tensile strain of several %, and the thinner the thickness, the more synergistic the microstructure and the surface effect are, the faster the destruction occurs.

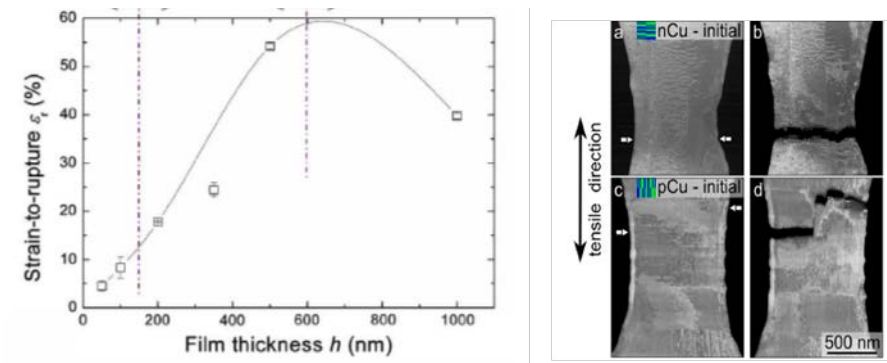

Figure 2.8 (a) Thickness dependent failure behavior of Cu thin film[10] (b) failure of the free standing Cu thin film. The smaller the thickness, the faster the rupture occurs. [11]

2.2.2. Stretchability of thin metal film on polymer substrate

As described above, the metal thin film is not inherently ductile, which is due to the instability of the material as well as the fine microstructural effect due to the thin thickness, as well as maximizing the surface effect. Therefore, researchers have devised a method for solving the instability of materials at the system level for the ductile behavior of the thin film. As a result, a study has been made on a composite system of metal thin film-polymer substrates[19] (Figure 2.9).

The principle that the polymer substrate solves the instability of the metal thin film is as follows. First, since the thin film and the substrate are deformed together, the stress applied to the system is prevented from concentrating only on the metal thin film. In addition, since the thickness of the polymer substrate is much thicker than the thickness of the thin film, a large amount of stress is used to deform the polymer substrate to help disperse the stress on the thin film. Also, unlike metal thin films where local stress concentration occurs, the polymer substrate helps to relieve locally generated stress because all parts are deformed uniformly according to the characteristics of the polymer. Finally, since the metal thin film is constricted by the polymer substrate, even if plastic deformation, in other words, necking occurs in the metal thin film, sufficient space for necking deformation is not provided, so that necking propagation is suppressed and fracture due to necking is retarded.

Also, the adhesion between the metal thin film and the flexible substrate should be excellent. In addition to the interfacial energy generated by the encounter of different dissimilar materials, the mechanical properties of the two materials differ, and when the deformation is applied, the behavior of the metal thin film is peeled off from the polymer substrate. When the delamination occurs, the delaminated portion exhibits the behavior

of the free standing film which does not enjoy the substrate effect at all and causes rapid breakage of the film. Therefore, the mechanical behavior of the metal thin film-polymer substrate has been actively pursued by the adhesion force. T. Li showed that when the perfect adhesion is established, the metal thin film can be deformed to the tensile limit of the polymer substrate without cracking by FEM simulation[20] (Figure 2.11).

These studies show that the metal thin film, which breaks even under a tensile strain of several percent, behaves with a large number of fine cracks on the surface instead of fracturing even under tens tensile strain[10]. The generation of cracks was suppressed as the thickness of the thin film was increased, the modulus of the polymer substrate was increased, and the additional bonding surface was added to improve the adhesion. Copper thin film - polymer substrate composites with Cr adhesion layer on copper 1 um film were deformed by 50% strain without deteriorating electrical properties[72] and Ni thin film was deformed without breaking even up to 100%[73].

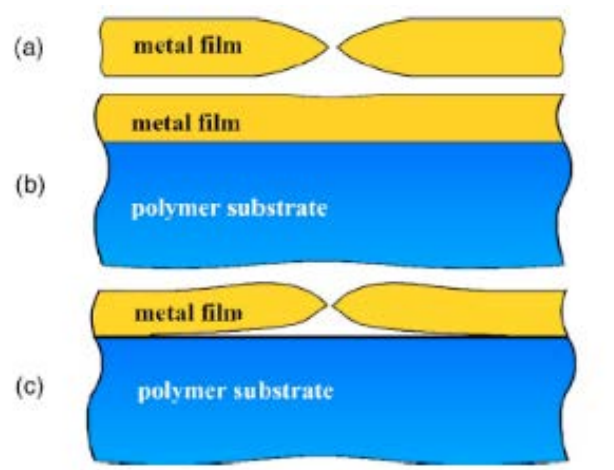

Figure 2.9 Schematic of the failure of (a) free-standing metal thin film (b) metal thin film on polymer substrate and (c) delaminated metal thin film from polymer substrate.[19]

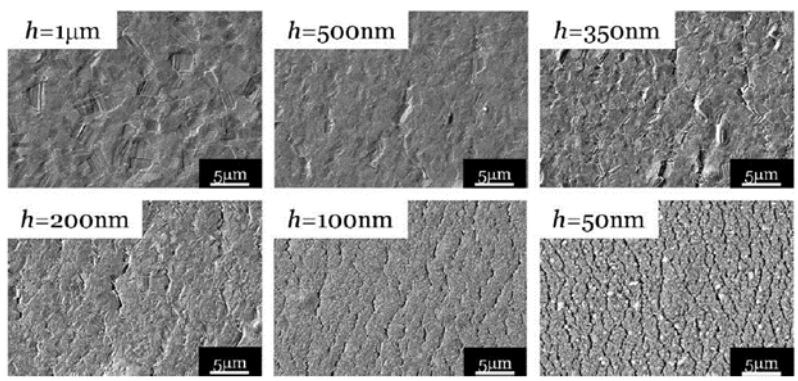

Figure 2.10. Typical cracking behavior and thickness effect of cracking of Cu thin film[10].

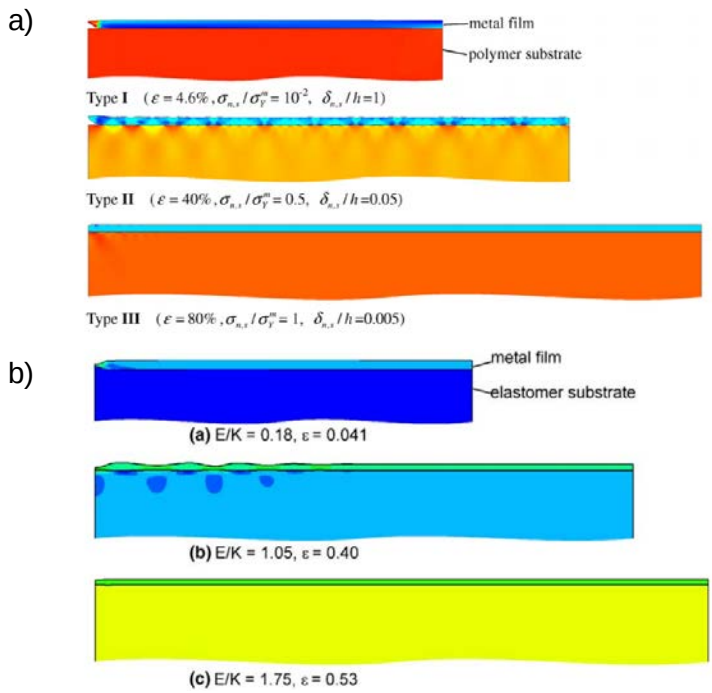

Figure 2.11 Simulation works a) varying adhesion[19] and b) varying elastic modulus and thickness[20].

CHAPTER 3

Experimental procedures

3.1. Sample preparation

To unveil the deformation behavior of Cu thin film, copper thin films were deposited onto polyimide substrates using thermal evaporation. Before copper film were deposited, polyimide substrates were washed to remove any dust and chemical residues on the surface. Polyimide substrates with thickness of 125 μm (Kapton® HN, Dupont) firstly were washed with ethanol, acetone, and isoprooply alcohol, sequentially, and then dried at room temperature. The thickness of Cu was 100 nm. Cu was deposited by thermal evaporation. The base pressure was 2×10^{-6} torr, and the deposition rate was 8 Å/s.

To compare the effect of electron beam irradiation in a same tensile testing, Cu thin film was deposited as a shape of square pads with assisted by metal shadow mask. Figure 3.1. shows an scanning electron microscope image of the total view of the sample. The size of each square was 100 μm × 100 μm. Electron beam irradiation was conducted in scanning electron microscopy (Inpect F, FEI) prior to tensile testing. The way to

irradiated electron beam on the Cu pad was, magnifying one copper pad to fulfill the scanning area (magnification: 2000×), focusing the copper pad, and scanning the image of Cu single pad for a long time. The acceleration voltage was changed from 3 kV to 30 kV, and irradiation time was 10 min, respectively. Spot size was fixed to 6.5 and working distance was fixed to 15 mm. Details of irradiation conditions are in Table 3.1.

After irradiation, polyimide film was stretched wit in-situ tensile machine (FN200, DEBAN) with strain rate 0.05^{-1}mm.

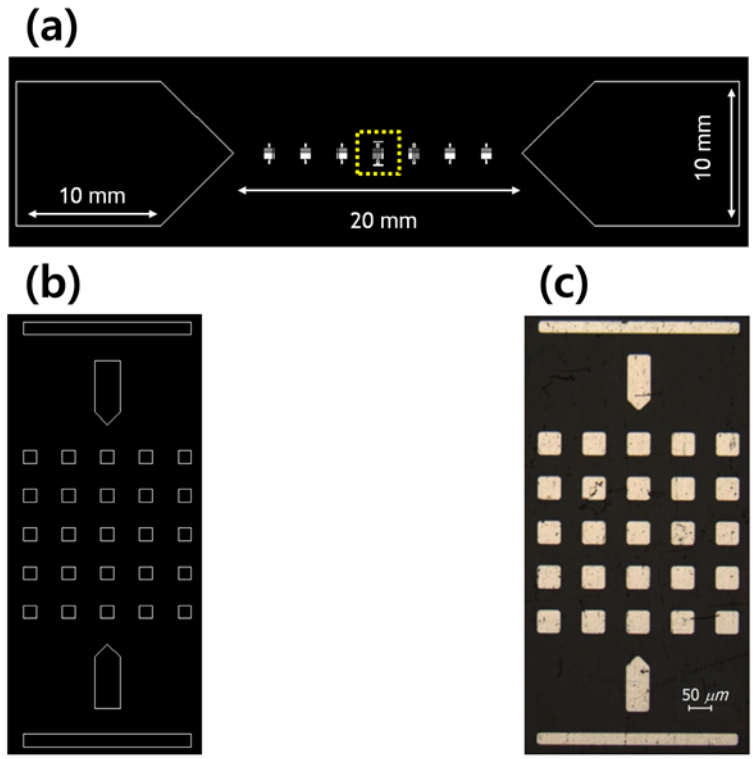

Figure 3.1 (a) Blue print of the shadow mask for the patterning of the array of Cu thin film pads was designed using 3D auto CAD. (b) Magnified pattern of the Cu pads array (yellow rectangle in Figure a). (c) Optical microscope image of the as-prepared Cu pad array deposited on the PI substrate.

acceleration voltage	0 – 30 kV
probe current	10 – 45 nA
irradiation time	10 min
electron density	8.33×10^{20} – 3.75×10^{21} /m^2

Table 3.1 E-beam irradiation conditions performed using FE-SEM.

3.2. Microstructure analysis

3.2.1. Investigation of microstructural changes in small grain

The most conventional method to investigate the microstructure of the metal is electron backscatter diffraction analysis (EBSD). EBSD is a very powerful method to characterize microstructure and crystallographic properties of materials.

When electrons are injected to material, some of them are transmitted through sample, while others generates secondary electron from sample or are scatted by collision with materials. These scatted electrons generate some patterns due to orientation of material, and EBSD is the technique to gather and transfers the pattern, known as Kikuchi pattern, into crystallographic characterizations of materials. Because it requires electron beam, EBSD is often conducted in scanning electron microscopy.

Figure 3.2(a) is a typical result from EBSD analysis of coarse grain copper. The thickness of copper sample was 1 μm deposited on polyimide substrate by thermal evaporation[74]. The image contains crystallographic orientation of each grain with different color. The texture and grain size of copper could be easily identified thorough the image. Relying on its convenience, EBSD has been use as one of the powerful analytic tool to investigate microstructure of material.

As the scale of material shrinks to nano scale, the grain size of thin metal film follows the thickness of the film, in other words, the grain size are smaller than submicron. Because the grain size becomes smaller, more fine resolution is required to analyze the microstructure of materials. However, the resolution of EBSD is ~ 300 nm, when the condition of sample and align of the beam is in the best. Figure 3.2(b) is a result from EBSD analysis of ultrafine grain copper. The thickness of copper was 200 nm, therefore

grain size was similar to a few hundred nanometer. It is hardly to distinguish the grain through figure 3.2(b), even, it seems like that the data is a noise. The reason is that, fine grains has a lot of grain boundary, and grain boundary often acts as the defects, i.e., the obstacle of electrons when electrons are injected and moved into the materials. Therefore signal of backscattered electron are severely interfered. To minimize the interference of signal, backscattered electron requires more energy to come out from materials. Also, compared to bulk material, film has much smaller interaction volume due to its constraint dimenssion in one direction. It means that, the signal is very week due to the small amount of atoms in the sample.

Therefore the energy of irradiated electron beam must be increased to acquire sufficient signal from the material with nanoscale. However, due to the limit of electron beam source, 30 kV is the limits of conventional scanning electron microscopy and it is inefficient to give enough enegy to backscattered electron. Hence the new analytic tool for investigating microstructure of ultrafine and nanocrystalline material which has a resolution with nanometer scale is required.

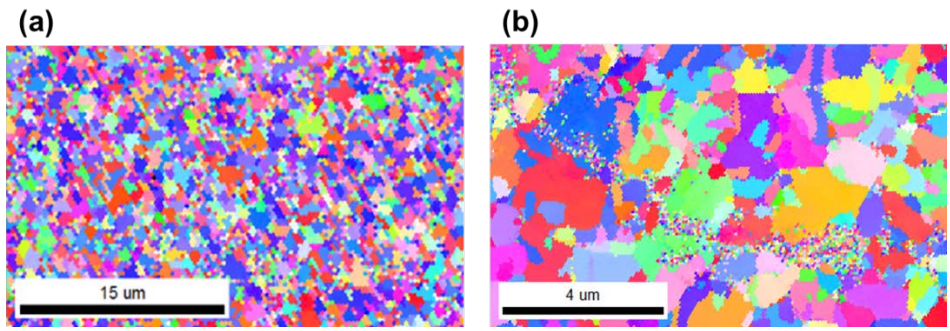

Figure 3.2 Invert pole figure of (a) ultrafine grain (film thickness: 200 nm) and (b) Coarse grain copper (film thickness: 1 μm) from EBSD. It is hard to distinguish individual grains in the scan image of ultrafine grain.

3.2.2. Operating principles of ASTAR™

ASTAR™ is the method to investigate ultrafine grained and nanocrystalline materials based on transmission electron microscopy. Contrary to EBSD, electron in ASTAR™ can have much higher energy due to higher acceleration voltage. The acceleration voltage is enlarged to hundreds of kilovolts.

The major difference between EBSD and ASTAR™ is, not only the acceleration voltage of electron beam, but also basement for analysis. ASTAR™ is based on the diffraction pattern generated from scattered electron while EBSD is based on the diffraction pattern generated from backscattered electron. One of the famous analysis by TEM is using diffraction pattern to figure out the orientation of materials. When electron collapsed with the material, it is diffracted with some oriented path depends on the orientation of the atom in the material, and diffracted electrons generates dot patterns. Each spot in diffraction pattern indicates the orientation of the materials, therefore crystallographic orientation could be acquired by analyzing the diffraction pattern.

ASTAR™ does same analysis as diffraction pattern-based analysis. The only one difference is that, electron beam in ASTART™ could scan the sample, in other words, electron beam moves around the sample automatically, and while scanning, electron beam is slightly tilted and rotated to do precision behavior. The principles of ASTAR™ is clearly described in Figure 3.3. The reason for precision is that, because even acceleration voltage is increased, the amount of signal is insufficient if the sample is very small. Therefore to gather a lot of signal, electron beam slightly tilted to enlarging the scanning area at one spot. As the precision angle increases, the amount of diffraction pattern increases, but it also require a lot of effort to analysis therefore precision angle is often used between 0.5 to 2 degree.

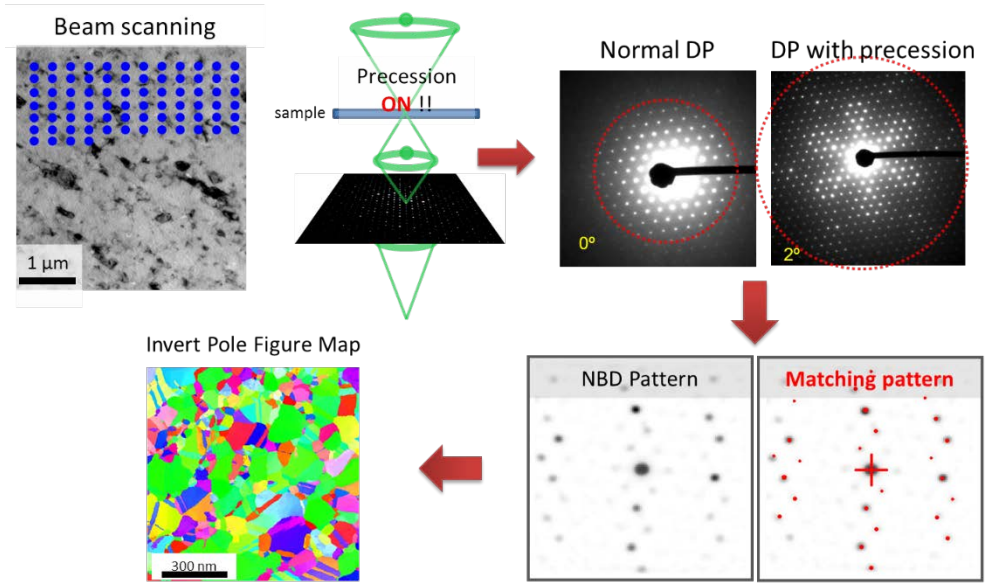

Figure 3.3 Illustration of the principle of ASTAR™. Electron beam scans the sample with precession to acquire the diffraction patterns. After matching the patterns with crystallographic orientation, invert pole figure map is acquired.

3.2.3. Set-up used in this study

Because the sample for ASTAR™ must be thin enough to penetrate electron beam, polyimide film under copper thin film must be removed. Hence, polyimide film was grounded by mechanical polishing, followed by fine ion beam milling. The source of ion beam was Ar, and the energy was 8V. Ion beam milling was conducted when the hole was generated on the sample. Copper film near the hole had almost no polyimide and also thickness of copper was thinner than 100 nm.

The ASTAR™ analysis was conducted in Tecnai F20 (Hitachi, Japan) in Korea Institute for Science and Technology (KIST). The acceleration voltage of injected electron beam is 200 kV and precision angle was 0.5 degree. The size of scanning area was 1 μm × 1 μm, and scanning resolution was 2.5 nm.

CHAPTER 4

Fabrication of highly reliable Cu thin film for flexible device

4.1. Introduction

Crack is the beginning of the separation of the material due to breaking of the bonding of atoms under the action of stresses, leading the failure of materials. Therefore most of studies related to crack has been focused how to prevent the formation and the propagation of crack on materials. In particular, the development of flexible device which is exposed on continuous mechanical deformation directly hence is more easier to failure due to formation of crack drives the researches to concentrate how to suppress the crack. However, recently researchers has started to use the crack as “benign” tool rather regarding the crack as the “problem” due to the following properties of the crack: the width of crack can be controlled to subnanometer, the nucleation of crack is spontaneously occurred when the stress is applied which is just a simple manner, and it is easy to scale up the formation and amount of crack. To utilize these properties of crack, the formation techniques of crack which is based on the difference of thermal expansion

coefficient of two materials in case of the formation of anisotropic crack, which is based on the photolithography or nanoindentor to design the starting point and ending point of crack in case of the aligned crack, which is based on the insertion of interlayer in the base material to change the path therefore to change the shape of the crack, are actively studied. Based on those techniques, crack is now used as a passage of the fluids in the nanofluidics field[75, 76], patterning template for metal deposition in nanopattering field[77-81], active material for strain sensor which the resistance of metal increases when the strain is applied therefore the cracks are opened, and vice versa[82,83].

Here, we introduce the novel and simple technique to control the area where crack would be formed by suppressing the formation of crack on copper film, based on electron beam irradiation that enhanced the adhesion between copper and polyimide substrate at the irradiated area. Using scanning electron microscopy, when the electron beam was irradiated on the Cu thin film with the thickness of 100 nm, there was almost no crack formation of Cu even under 30 % tensile strain. This is due to the enhancement of adhesion strength between Cu and polyimide, verified by nanoscratch test. We also found that the hardness was increased in polyimide after electron beam irradiation. It implies that the further polymerization induced by electron beam drives the enhancement of adhesion. We also bound that there is a threshold in acceleration voltage of electron to penetrate copper film and reach to the polymer substrate by both experiment and Monte-Carlo simulation, and the value was 5 kV. Crack patterning due to electron beam irradiation is mask-free therefore it is facilitate to control the area where crack must not be generated in a simple and easy manner. Further, the electrical property, in other words, conductivity of the Cu film is decreased when the crack is formed, so we could import the contrast pattern of electrical conductivity on the copper by just simple mechanical deformation. Based on those expert properties, we fabricated organic

light emission diode (OLED) which was automatically patterned emission area by deforatmion. Through this, we see the possibility to use our electron beam patterning technique as the formation technique for further flexible PCB and strain-responsive device.

4.2. Experiments

Copper thin film was deposited onto polyimide substrate by thermal evaporation and electron beam irradiation was conducted in scanning electron microscopy. The deposition conditions and irradiation conditions described in **Sec. 3.1**.

In case of fabrication of OLED, Cu thin film was deposited on PI with thickness of 100 nm for bottom electrode, then electron beam was treated with smile pattern. After irradiation, OLED materials (HATCN (10 nm); NPB (40 nm), CBP:Ir(ppy)^3 (20 nm); BCP (15 nm); Alq3 (25 nm)) was thermally deposited on Cu electrode. Finally, transparent metal electrode (LiF (0.5 nm); Al (5nm); Mg:Ag (2:1) (20 nm)) was thermally deposited on OLED and OLED device was stretched up to 7 % tensile strain. The fabricated device had a width of 1.5 mm and a length of 1 mm.

4.3. Elongation of Cu thin film without crack up to 30 %

A schematic of the process is described in Figure 4.1(a). A single Cu pad was irradiated by the electron beam prior to tensile testing (acceleration voltage: 30 kV, probe current: 10 nA, irradiation time: 10 min) then Cu pad had a tensile strain up to 30 %.

Figures 4.1(b) – (f) show the surface morphology of the untreated and electron beam treated Cu pads during tensile testing using a micro tensile machine in the vacuum chamber of a FE-SEM. The untreated Cu pad (Figure 4.1(b)) was severely damaged by cracks and delaminated during tensile testing. This morphological change is consistent with the results from previous studies on the deformation of Cu films on PI.10 In general, above a critical strain, metal films on a polymeric substrate eventually rupture due to either strain localization or debonding from the substrate. However, the surface morphology of the electron beam treated Cu pad after tensile testing (Figure 4.1(c)) exhibited significantly reduced microstructural damage (i.e., shorter and narrower cracks than those found on the untreated sample). In addition, the majority of the damage consisted of locally formed microcracks or voids, which were not connected to each other.

To the further extend, the cracking morphology on Cu thin film can be effectively controlled by electron beam patterning. After electron beam was intentionally irradiated on half of a single Cu pad, the Cu pad was elongated by a strain of 30% as shown in Figure 4.1(d) and 4.1(e). Interestingly, clear differences in the density of cracks across the boundary between the untreated and electron beam treated region were observed. Only irradiated area had no crack on Cu surface during tensile deformation whereas non-irradiated area showed usual crack behavior of Cu thin film.

The areal selectivity of electron beam irradiation was further investigated using a more intricate pattern (i.e., the letter “KIST”) (Figure 4.2). Alphabet “S”, which has the curviest shape and alphabet “T” are clearly patterned on Cu by using imaginary mask in Figure 4.1(f). It is important to note that the probe current applied for the treatment of “S” and “T” was 45 nA with an acceleration voltage of 25 kV to fix the power ratio of the electron beam/irradiation area. After tensile deformation with a strain of 30 %,

significant cracking and delamination were observed in the untreated region. However, the electron beam treated region exhibited no remarkable cracks, and the “S” and “T” shape were well maintained and clearly distinguishable from the untreated region.

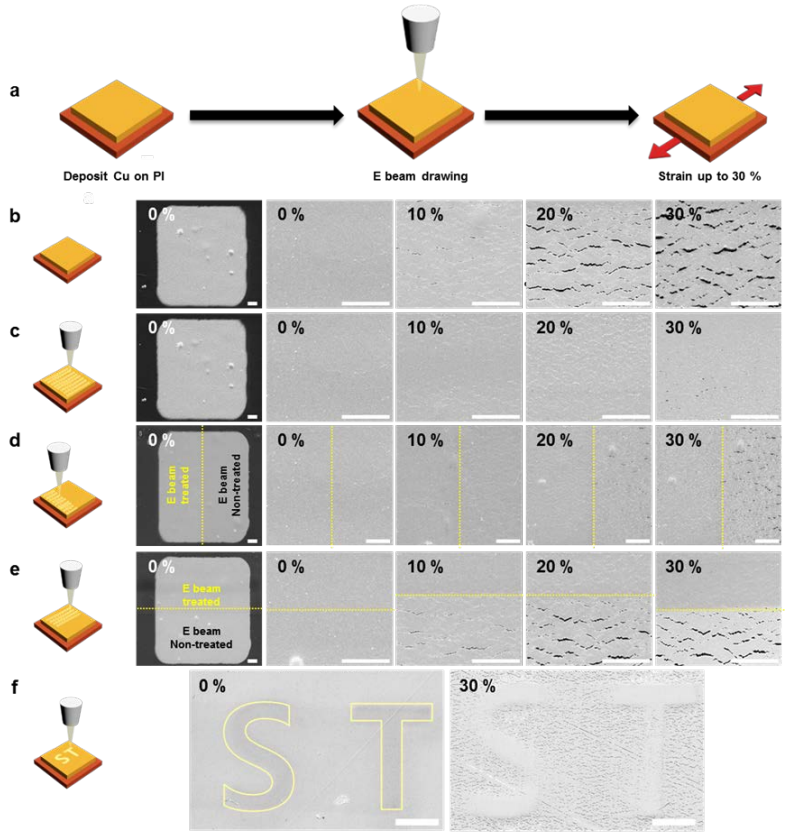

Figure 4.1 FE-SEM images of Cu thin films deposited on a PI substrate during tensile deformation at a strain rate of 0.05 min^{-1} without irradiation (b) and after irradiation (c), respectively. Areal selectivity and patterning capability of electron beam irradiation. FE-SEM image of strained Cu films, where only the right half (d) and top (e) of the film was irradiated with the electron beam. (Electron beam irradiation conditions for Figures 4.1b - e: acceleration voltage of 30 kV, probe current of 10 nA, and irradiation time of 10 min) (f) FE-SEM images of Cu films with the letters “S” and “T” patterned by selective electron beam irradiation after straining up to 30 %. (Electron beam irradiation conditions: acceleration voltage of 30 kV, probe current of 45 nA, and irradiation time of 30 min). Scale bars, 10 μm.

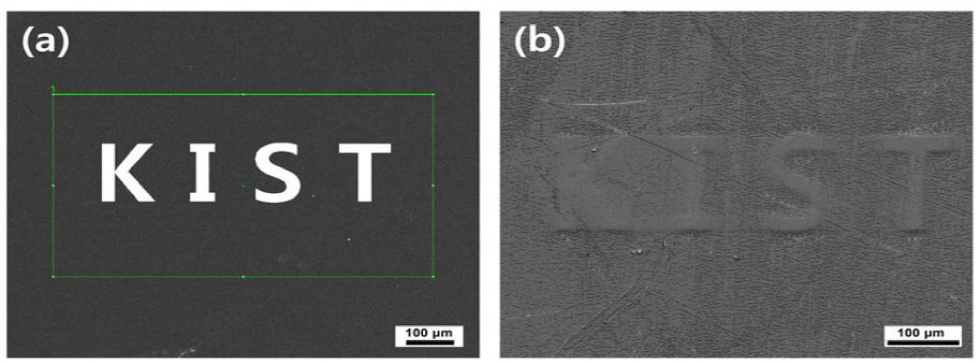

Figure 4.2 (a) Patterning of the "KIST" letters using FIB with selective e-beam irradiation (the white letters are the imaginary mask for patterning). (b) FE-SEM images of the Cu films with the "KIST" lettetrs patterned by selective e-beam irradiation after tensile deformation of 30 %.

The behavior of cracking can be controlled cooperatively by acceleration voltage. Figure 4.3(a) shows surface morphology of Cu 100 nm film on PI varying acceleration voltage from 3kV to 30 kV, and strain on Cu was 25 % same for all Cu films. As shown in figure, crack density was not changed when the acceleration voltage was lower than 5kV.

However, when the acceleration voltage was increased beyond 5kV, the crack density was continuously decreased. Figure 4.3(b) quantitatively elucidates the variation in the crack density as a function of the acceleration voltage of the electron beam. The relative crack density is defined as D/D_0 (%), where D and D_0 are the crack density of the electron beam treated and untreated (0 kV) Cu pads, respectively. The crack density was calculated by dividing the integrated area of the cracks by the area of the entire Cu pad. The detailed image processing for the calculation is shown in Figure 4.4. In case of acceleration voltage below 5 kV, crack density was not changed. The crack density started to decrease at an acceleration voltage of 5 kV (by ~ 20 %) and then went further down by ~80% at 30 kV. The result of surface morphology and crack density mean that, 5kV is a threshold voltage value. Also it could be speculated that kinetic energy of electron is the major factor of changing properties of materials.

.

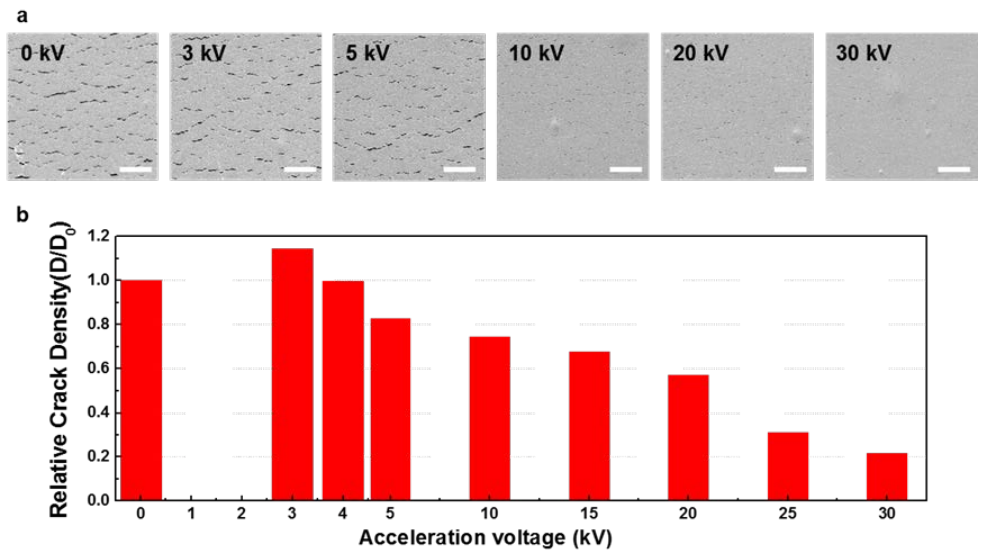

Figure 4.3 (a) Surface SEM images of Cu thin film varying acceleration voltage from 0 kv to 30 kV. As acceleration voltage increases, crack density decreases after 5 kV (b) Relative crack density (D/D0, where D and D0 are the crack density of the electron beam treated and untreated (0 kV) Cu pads, respectively) as a function of acceleration voltage after strained up to 25 %. Scale bars, 10 μm.

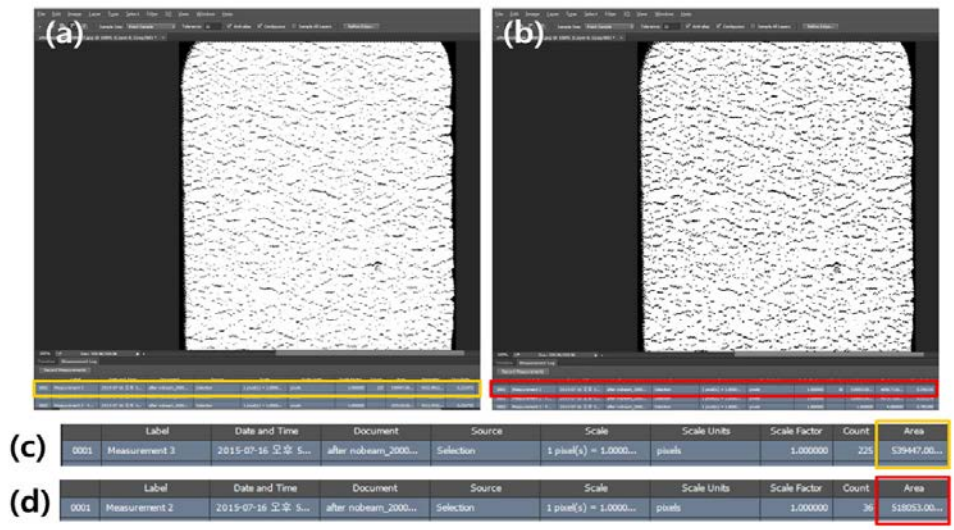

Figure 4.4. Example of the procedure for calculating the areal density of cracks using the Photoshop software. (a) SEM images converted to grey scale and the calculation of the total area of strained Cu pad using the selection tool. (b) Calculation of the area covered by Cu (white region) using the magic wand tool. (c) Quantification results of the area of the total pad (c) and Cu only (d). The areal density of cracks was calculated as (area of total pad (c, yellow rectangle) – area of Cu (d, red rectangle))/area of total pad.

4.4. Enhancement of adhesion through electron beam irradiation

4.4.1. Electron trajectory simulation

In order to see how the electron beam causes a change in the material and suppress the cracking of the copper film, we first checked the behavior of the electron beam in the material through Monte Carlo simulation using Carlo simulation software (CASINO 3.3.0.4, Universite de Sherbrooke, Canada[84]). Figure 4.5 shows a three dimensional view and cross-section view (XZ) schematic of the sample, electron beam position, and analyzed volume. A cartesian distribution was used to calculate the cartesian distribution over a width, height and depth of 1000 nm, respectively; the step size was 2 nm for both directions. An acceleration voltage of electron beam were 4, 5, 10, 15, 20, and 25 keV beam energy and diameter of electron beam was 1 nm beam. Total of 10,000 electron trajectories were simulated.

Figure 4.6 shows the electron path and the energy change of the electrons by varying the acceleration voltage to 4-25 kV. The energy of the electrons is absorbed entirely by the copper thin film up to the acceleration voltage lower than 5 kV, and electrons reach the PI from the accelerating voltage of 5 kV or more through the copper thin film. From this simulation, it can be seen that the energy of electrons is transferred to copper and PI according to the accelerating voltage, so that copper and PI can be influenced by electron beam irradiation. Figure 4.7(a) is a graph showing the amount of kinetic energy of electrons absorbed by copper according to the acceleration voltage, and Figure 4.7(b) is a graph showing the ratio of electrons passing through copper according to the acceleration voltage. As shown in Fig. 6, there is no electron to be transmitted at an acceleration voltage lower than 5 kV, and most of the energy of electrons is absorbed by

copper. It can be also seen that the energy absorbed by copper decreases as the number of electrons transmitted increases at an acceleration voltage of 5 kV or more.

Based on the above simulation results, the possibility of material change by electron beam is as follows. First, when the nature of the metal is changed by electron beam irradiation, an electron beam having an energy of several MeV or more is irradiated and the metal is deformed by the heat generated at this time, or by depositing a metal on the non-conducting material so that electrons irradiated onto the metal cannot escape and accumulate, and then the metal is deformed in such a manner as to cause diffusion of metal atoms through the generated electric field[85-89]. Considering the possibility of deforming the metal in this way based on the simulation results, it is impossible for the deformation of the metal due to heat because the energy absorbed through the electron beam irradiation in this study is only a few keV. It is also expected that electrons will not accumulate on the metal film and will not be deformed by the electric field.

On the other hand, in the case of a polymer material, studies have been actively conducted to change the mechanical properties and morphology of a polymer by breaking bonds between atoms in the polymer through electron beam irradiation to form radicals and causing polymerization or carbonization through the formed radicals[90-95]. In addition, when polymers are used in combination with other materials, these radicals can be used not only to polymierzation but also to create new bonds with atoms of other materials, so that electron beam / ion beam irradiation is also used to improve adhesion between dissimilar materials. Particularly, in the case of polyimide, research has been carried out to induce polymerization through radical formation by cutting C = O bonding through electron beam / ion beam irradiation. It is known that the bonding energy of C = O is 7.78 eV[96], which is very small compared to the electron beam energy normally irradiated, so that deformation by the electron beam occurs easily. Based on the above

phenomenon, Monte Carlo simulation results show that electrons with an acceleration voltage of 5 kV or more reach the PI through the copper thin film, as shown in the result of Figure 4.6. Figure 4.8 shows the energy distribution of the electrons passing through copper, that is, the distribution of the energy of the electrons incident on the PI by acceleration voltage. As shown in Figure 4.8, it is expected that the energy possessed by the electrons will be almost equal to the acceleration voltage, and that the higher the acceleration voltage, the more the primary electrons can penetrate, therefore more secondary electrons will be generated. Thus, it can be expected that the transmitted electrons and secondary electrons will cause PI or interface deformation through radical generation. In addition, it can be expected that the effect of electron beam will not occur at an acceleration voltage lower than 5 kV because an acceleration voltage of 5 kV or more is required for the electrons to reach the PI.

Based on the above simulation results, we tried to confirm the influence of the electron beam on the material by dividing it into three parts: copper, interface between copper and PI, and PI.

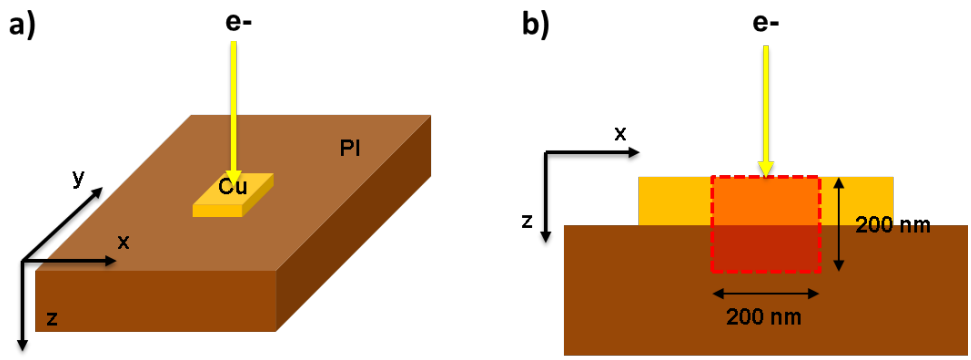

Figure 4.5 a) Three dimensional view and b) Cross-section view (XZ) schematic of the sample, electron beam position, and analyzed volume for simulation.

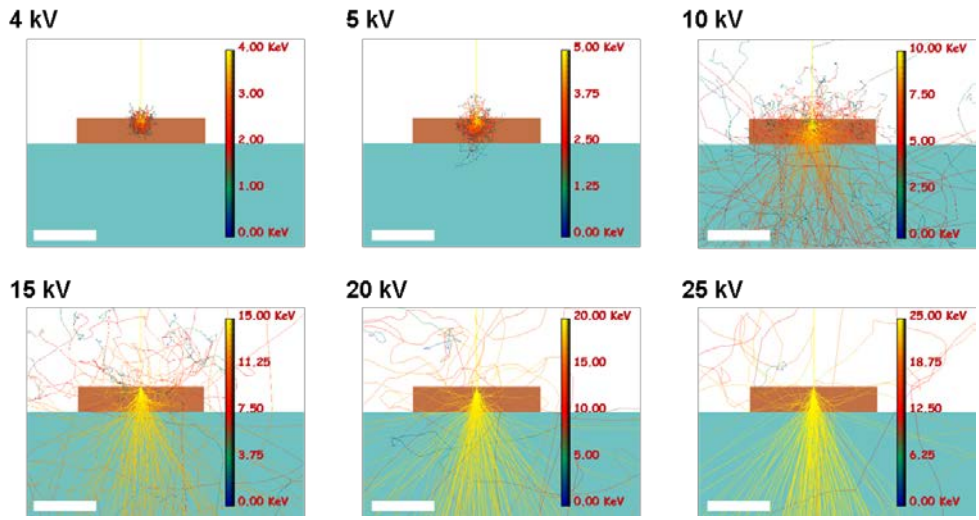

Figure 4.6 Electron trajectory simulated by Monte Calro simulation (CASINO software) striking Cu 100 nm film with PI substrate. Electron could penetrate Cu film with acceleration voltage above 5 kV.

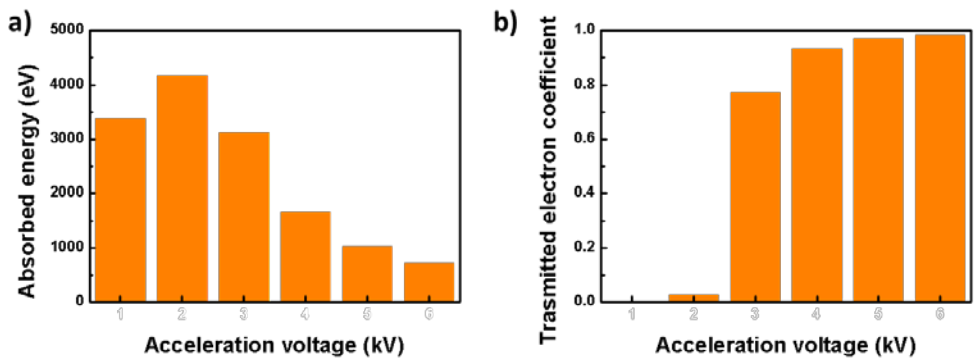

Figure 4.7 Electron trajectory simulated by Monte Calro simulation (CASINO software) striking Cu 100 nm film with PI substrate. Electron could penetrate Cu film with acceleration voltage above 5 kV.

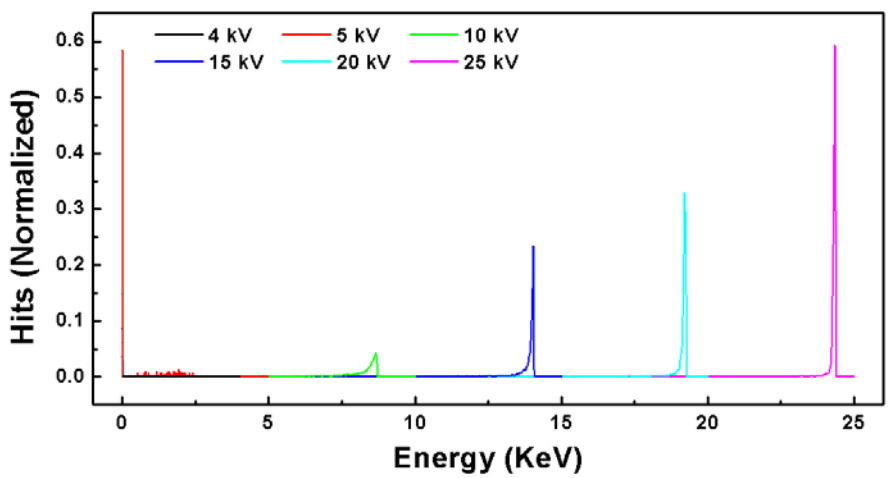

Figure 4.8 Electron trajectory simulated by Monte Calro simulation (CASINO software) striking Cu 100 nm film with PI substrate. Electron could penetrate Cu film with acceleration voltage above 5 kV.

4.4.2. Electron beam effect on Copper

It should be noted that electron beam does not change microstructure of Cu thin film. In other words, electron beam does not change the mechanical property of Cu, which is closely relate to microstructure. To verify electron beam effect on Cu, ASTAR™ analysis was conducted. Because thickness of 100 nm is much smaller than resolution of EBSD, it is impossible to scan nano-sized grains and their orientation by EBSD. Contrary to EBSD, resolution of ASTAR™ is few nanometers. (Approximately 2 nm) (ref) Therefore we could observe the grains and orientations of 100 nm film by using ASTAR™ and this is the first result of microstructure of metal thin film on polymer substrate. Figure 4.9(a) and 4.9(b) are inverted pole figures of non-treated and treated Cu film and texture map of each Cu is included. It is revealed that Cu thin film deposited on PI substrate had random texture. Also, comparing the Cu texture before electron beam irradiation and after electron beam irradiation, Cu still had a random texture even after electron beam irradiation. In addition, it seemed that grain size of Cu had not changed after irradiation. Figure 4.9(c) is quantitative analysis of grain size distribution of Cu before and after irradiation. It is discovered that Cu thin film deposited on PI had a lot of tens-of-nanometer sized grains and few submicrometer grains and it seems that the difference in distribution before and after irradiation of electron beam is almost unchanged. In addition, length of grain boundaries and twin boundaries in scanned region is measured and results are in Figure 4.9(d). As shown in Figure 4.9(d), there is little change in the length of each boundary before and after irradiation. All these aspects represent that electron beam did not change the microstructure of Cu.

Considering that the microstructure is closely related to the mechanical properties, it is figured out that electron beam did not change the mechanical properties of Cu. That

is to say, it is figured out that inhibition of crack nucleation and propagation by electron beam is caused by other aspects rather than change of ductility of Cu.

Interestingly, as in 3a and 3b, Cu thin film deposited by thermal evaporation had a lot of nanotwin. Thickness of twin lamella varies from 2 nm to 20 nm. It is well known that Cu with nanotwin has good ductility (up to 15 %) strain in bulk material[13]. However, contrary to bulk Cu, crack initiated at 5% strain on nanotwinned Cu thin film, which is usual crack initiation point of Cu film on polymer(ref). It elucidates there is no enhancement of ductility caused by nanotwin in film system. Instead, strain localization strongly dominates failure of Cu film on polymer system by delamination and necking of film. Therefore interface property between Cu and PI much more important to improve ductility of Cu thin film rather enhancement of mechanical property of Cu itself.

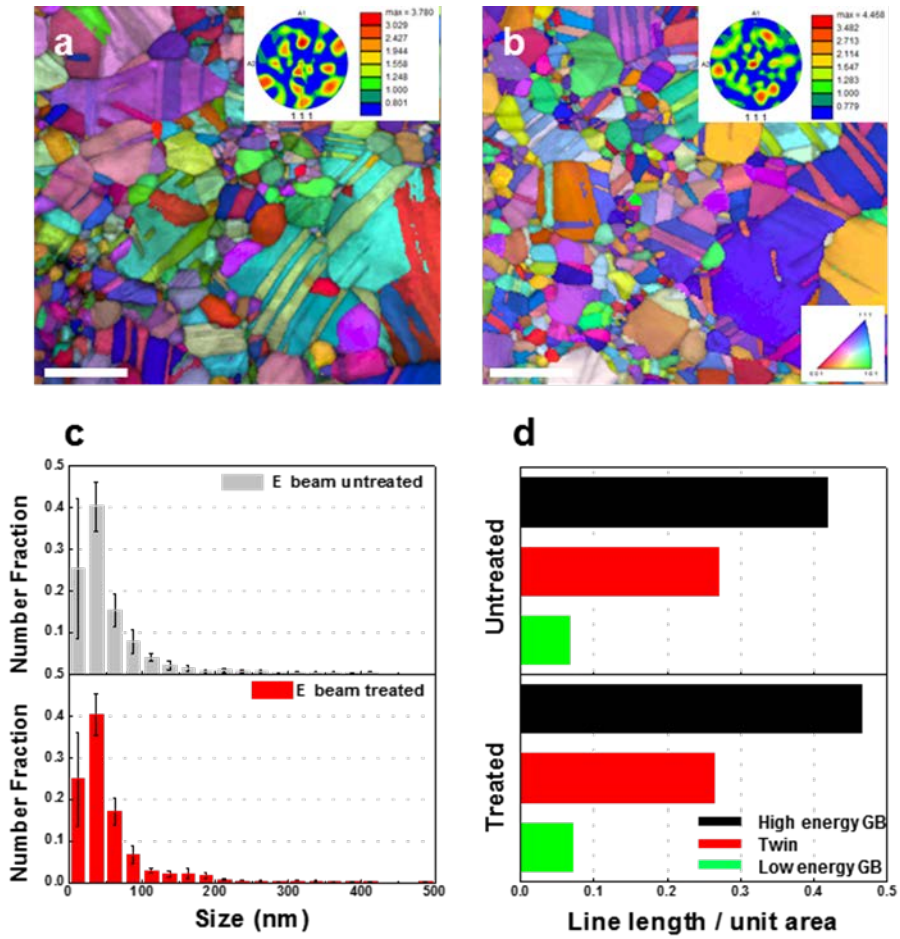

Figure 4.9 ASTAR™ analysis for investigating electron beam effect on Cu ASTAR™ inverted pole figure of (a) electron beam untreated and (b) e- beam treated Cu thin film. (Texture maps are included.) Both have no significant texture. (c) Grain size distribution and (d) misorientation faction. Both are also almost same. Scale bars, 200 nm (a, b).

4.4.3. Electron beam effect on Copper/Polyimide interface

The electron beam that reaches the PI through the copper can affect the copper / polyimide interface or the PI. First, EELS analysis was performed at the interface to see if the electron beam affected the copper / polyimide interface. Figures 4.10a and 4.10b show the HADDF image and EELS line profiles of the copper section samples without electron beam irradiation and with electron beam irradiation, respectively. As the arrow indicates, the distribution of copper and polyimide (identified by O and N) at the interface was checked to confirm that there was no intermixing layer due to diffusion of copper. In other words, no physical mixing occurred between the two materials.

Next, we examined the EELS spectrum of copper before and after electron beam irradiation to see if chemical bonding between copper and polyimide modified by electron beam can be formed as described in Section 4.4.1. This is because when copper makes chemical bonding with an element present in the PI, a new peak is expected to occur in the spectrum of the electron irradiated copper. However, there was no difference in the spectrum of both the untreated copper and the treated copper, indicating that the electron beam did not change the interface.

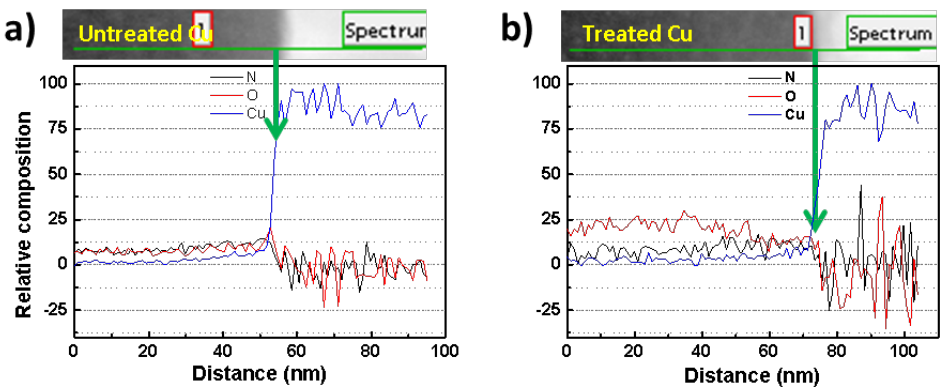

Figure 4.10 HADDF image and EELS line profile of nitrogen, oxygen, and copper of a) electron beam untreated sample and b) electron beam treated sample.

4.4.4. Electron beam effect on Polyimide

The damage resistance to tensile deformation of a metallic thin film deposited on a polymer substrate is strongly related to the interfacial adhesion strength. Previous studies have reported that structural modification of bonding nature in polymers (e.g., degree of crosslinking, chemical bonding or arrangement of the backbone chain) can be induced under e- or ion-beam irradiation and structural modification of PI after irradiation is clearly signified by increase of hardness.

As shown in figure 4, electrons could penetrate Cu with acceleration voltage higher than 5 kV. These penetrating electrons could modify the bonding of PI and lead to the formation of strong interfaces between Cu and the PI. In figure 4.11(a), hardness of Cu/PI and PI are measured before and after irradiation by nanoirradiation. After irradiation, hardness of PI increased from 0.39 GPa(±0.17) to 0.60 GPa (±0.15) and hardness of Cu/PI increased from 0.69 GPa(±0.32) to 0.89 GPa(±0.23). Interestingly, the differences of hardness before and after irradiation of each case is almost same. As shown in Figure 4.11(b), difference of PI is 0.22 GPa and difference of Cu/PI is 0.20 GPa. It indicates that electron beam changes hardness of PI only, not hardness of Cu.

It is well known that soft adhesive materials physically fasten two stuffs by stiffening itself. This is called as adhesive joining. (ref) While joining, adhesive materials fill interface completely and shape of interface is changed to wavy curvatures without any voids at interface. Figure 4c and 4d are cross section image of interface between Cu and PI before (Figure 4.11(c)) and after irradiation (Figure 4.11(d)). Morphology of interface between PI and Cu was flat before irradiation. However, compared with interface before irradiation, it is clearly revealed that shape of interface was changed after irradiation. Yellow arrows in figure 4d indicate curvatures in interface. Because interface with wavy

curvatures usually refers to adhesive joining, it could be inferred that PI works as adhesive materials by structural change under electrons beam penetrating Cu thin film and while bonding structure of PI changed, hardening is concurrently occurred. It is worth noting that hardening of PI works as adhesive materials only in case of composite system. When PI was hardened by irradiation before deposition of Cu, it did not show the adhesive behavior as in Figure 4.12.

The effect of adhesive joining is distinctly reveled in scratch test. Figure 4.11(e) shows critical normal force of non-treated and treated sample measured from nanoscratch test. Critical normal force is the normal force at first delamination of Cu, and it is proportional to interfacial adhesion strength. As shown in Figure 4.11(e), critical normal force was increased from 2.74 mN to 3.37 mN after irradiation. This indicates that it requires more stress to delaminate Cu from PI after e beam irradiation because adhesion strength is increased after electron beam irradiation. Critical normal force can be converted into work of adhesion using the following equation[97]

$$L_{crit} = \frac{d_{crit}}{\nu_c \mu_{crit}} (2tE_cW)^{1/2}$$

where L_{crit} is critical normal force, d_{crit} is scratch width, v is poisson's ratio, u is friction coefficient, T is thickness of film, E_c is Young's modulus of Cu, and W is work of adhesion. Remarkably, work of adhesion increased 1.5 times after irradiation, respectively. It clearly indicates that electron beam enhances adhesion between Cu and PI. Moreover, images after scratch test of electron beam untreated (Figure 4.11(f)) and treated Cu film (Figure 4.11(g)) showed different surface morphology. Compared to untreated Cu, treated Cu film showed much more stiff behavior because of enhanced adhesion.

The direct analysis of changing of PI is conducted by XPS analysis. As mentioned in Section 4.4.1, electron beam deforms PI due to polymerization caused by radicals generated from broken C=O bond. According to electron trajectory simulation, electrons accelerated with 25 kV could penetrate copper thin film and their energy is near 25 kV, we acquired C and O spectrum of untreated PI and treated PI with acceleration voltage 25 kV. As in Figure 4.13, after irradiating electron beam, amount of C=O bonding decreased while amount of C-O bonding increased. It confirms that transition of polyimide by electron beam irradiation could occur.

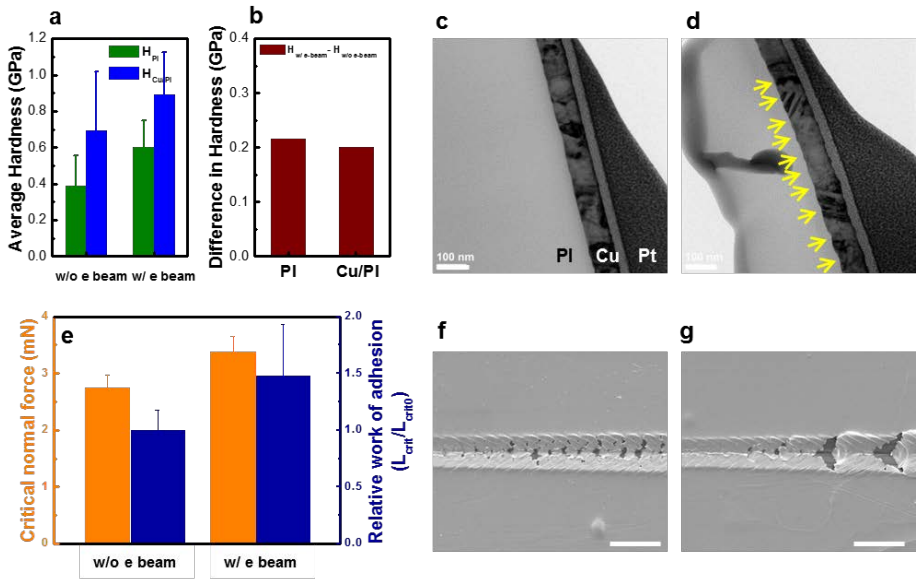

Figure 4.11 (a) Hardness of both untreated and treated sample by nanoindentation. (b) Difference of hardness before and after irradiation. Cross section image of interface of (c) electron beam untreated and (d) e- beam treated sample by TEM. (e) Critical normal force, normal force at the first delamination of Cu film from PI, is measured from both electron beam untreated and electron beam treated Cu. Relative work of adhesion (L_{crit}/L_{crit0}, where L_{crit0} is the work of adhesion of the electron beam untreated). Work of adhesion could be calculated by using critical normal force. SEM image of e- beam untreated (f) and e beam- treated (g) Cu thin film after scratch test. Scale bars, 100 nm (c, d); 50 μm (f, g)

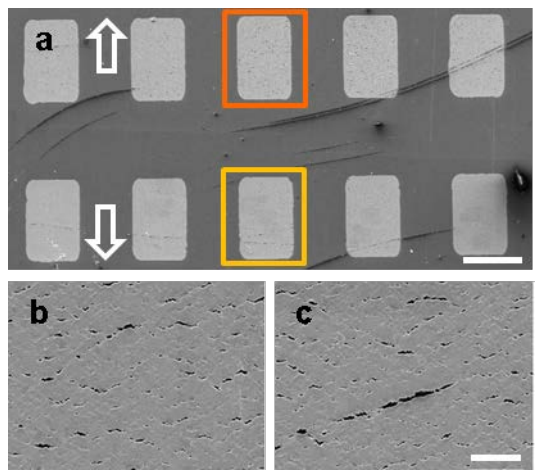

Figure 4.12 (a) Cu pad on polyimide substrate without any electron beam irradiation and (orange square) Cu pad on polyimide substrate which is irradiated by electron beam prior to the deposition of copper thin film (yellow square). (b) and (c) are the magnification of copper in orange and yellow square of (a), respectively. Scale bars, 100 um (a); 1 um (b)

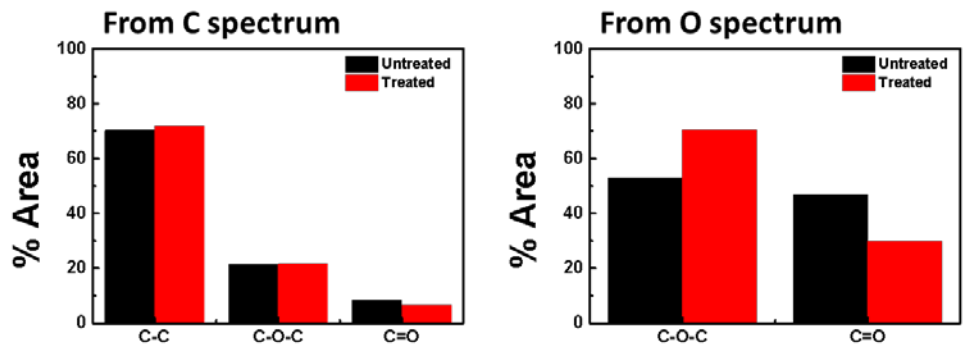

Figure 4.13 XPS result of C and O spectrum of electron beam untreated polyimide and electron beam treated polyimide. After electron beam irradiation, amount of C=O bonding decreased and C-O bonding increased.

4.5. Fabrication of strain-responsive OLED

Because crack is closely related to resistivity of metal, enhanced surface morphology improves electrical property of Cu thin film. The resistivity of the electron beam treated Cu thin film increased by one quarter of the resistivity of Cu before the tensile strain, but the resistance of the untreated Cu thin film was doubled. (Figure 4.14)

By combining features related to areal selectivity and preserving electrical property, a stretchable OLED with a rigid metal electrode was produced. As shown in figure 4.15, all areas were turned on before stretching under 8 V. A few dark spots were observed, but this was caused by intrinsic factors such as surface of PI and uniformity issue of deposition. OLED was retained for a 4 % strain. In 5 % strain, the luminescence was different in the smile-patterned area and the untreated area. Patterned area was brighter than untreated area. As tensile deformation was applied further, OLED on untreated Cu was gradually turned off, while OLED on smile-patterned Cu still maintained their initial brightness (figure 4.15(e) and 4.15(f)). Finally, at 7 % strain, OLED on untreated Cu was completely turned off and only OLED on patterned Cu was turned on (figure 5f). At this strain, brightness of OLED slightly decreased compared to initial status because resistivity of Cu was slightly increased during stretching. However, as previously mentioned, the resistivity change was much higher in untreated Cu compared to patterned Cu, therefore OLED on untreated Cu was completely failed while OLED on patterned Cu only lost only a small amount of its brightness.

This result Indicates two interesting aspects: First, since electron beam treatment can selectively change the resistance of a material, a device made of the same material can operate differently depending on whether the beam is irradiated or not. In figure 4.15(d) and 4.15(e), the OLED is illuminated in both the irradiated and non-irradiated regions,

but the brightness in non-treated region is low due to high resistance. In this way, the device can be manufactured much more economically because it can control the conductivity by changing the density of the crack through the electron beam in the same material, while making the device usually using materials with different conductivity.

Electron beam treatment also makes it possible to use metals even it is rigid for stretchable devices. Generally, conductive polymer or flexible carbon composite materials are widely used as an electrode or metallization of stretchable device. Since both materials have lower electrical conductivity than metal, high driving voltage is required to turn on the device. However, electron beam treatment can solve the electrical reliability issue by using a metal which has superior electrical property compared to other materials. Thus, this method can overcome the limitations of the application of metal to flexible devices.

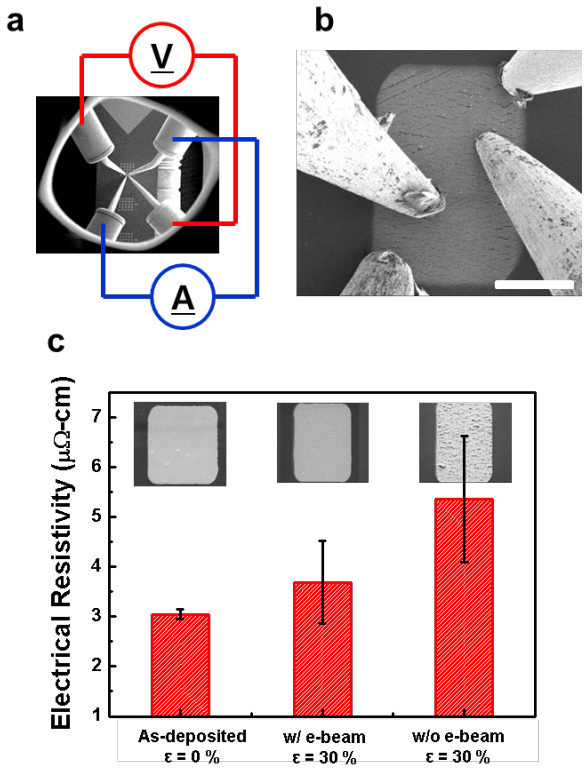

Figure 4.14 (a) Schmatic of in-situ sheet resistivity measurement and (b) FE-SEM images of the electrical resistivity measurement of e-beam treated films at a tensile strain of 30 % (E-beam irradiation condition: acceleration voltage of 25 kV, probe current of 10 nA, and irradiation time of 10 min). (c) Electrical resistivity of the as-deposited and strained (ε=30 %) Cu films with and without e-beam irradiation. Resistivity measurement of the strained Cu films was conducted using the 4 point probe method while maintaining the final strain using a tensile jig.

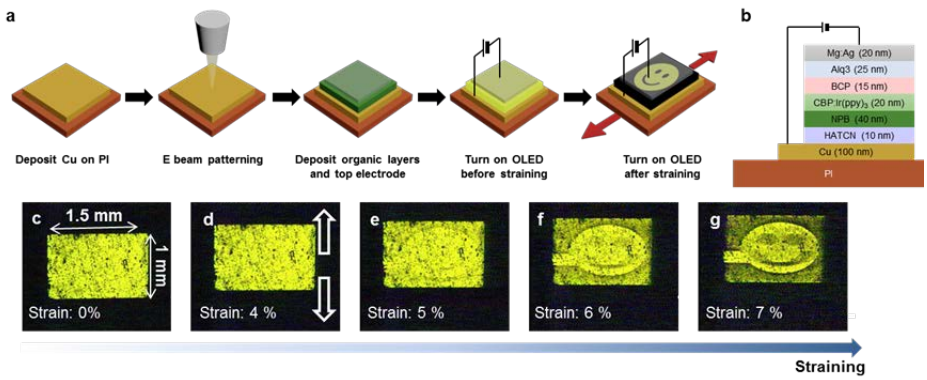

Figure 4.15 (a) OLED preparation: Cu 100 nm film for bottom electrode deposited on PI, then Cu is patterned with smile using FIB scanning. After patterning, active materials and top electrode are deposited on Cu. (b) Structure of OLED. Photographs of the stretchable OLED at 8 V with strain values of 0 % (c), 3 % (d), 3.5 % (e), 4 % (f), and 4.5 % (g). Scale bar, 500 μm.

4.6. Summary

In summary, the use of electron beam irradiation has been proposed to achieve exceptionally damage resistant Cu thin films deposited on a polymeric substrate, which are essential structures for constructing flexible systems utilized in future electronics, energy devices and sensors. In spite being extremely thin with a thickness of 100 nm, which is considered vulnerable to external deformation compared to thicker films, crack formation and delamination was effectively mitigated in the electron beam treated Cu films, even at a severe tensile strain of 30 %. The corresponding mechanism for the enhancement of mechanical stability was due to the formation of strong Cu/PI interfaces via hardening of PI by electron beam irradiation. In addition, the electrical conductivity of the electron beam treated films after tensile deformation was well preserved due to the higher degree of microstructural continuity and suppressed formation of defects. Furthermore, electron beam irradiation exhibited a high areal selectivity. Therefore, the application of this simple methodology can be further expanded to pattern-on-demand nano-patterning or the precise strength or crack density control and we demonstrate this probability by fabricating stretchable OLED with metal electrode on PI substrate.

CHAPTER 5

Deformation mechanism of Cu thin film under large tensile deformation

5.1. Introduction

The applicable range of materials is the same as the range in which the mechanism of the material is understood. The mechanical properties of the material are closely related to the microstructure of the material, and therefore the expansion of the understanding of the microstructure deformation mechanism is important because it leads to the expansion of the mechanical properties of the material. As a result, studies have been carried out to reduce the size of the material to an extreme level, or to increase the deformation applied to the material to an extreme extent and to grasp the mechanical properties while widening the scale of the deformation mechanism. As a result, from the viewpoint of the size of materials, the strength of material firstly increases due to suppression of movement of dislocation because of grain size is small (Hall-Petch relationship) and then decreases due to activation of grain-based deformation mechanism such as grain boundary migration, grain rotation, or grain boundary sliding.

(inverse Hall-Petch relationship) while grain size becomes smaller from coarse grain to nanocrystalline[17]. On the other hand, studies on recrystallization and recovery due to severe plastic deformation have been actively pursued from the viewpoint of deformation applied to the material[98-103], but studies on the microstructure deformation mechanism due to extreme tensile deformation have not been conducted. In contrast to compressive deformation, tensile strain is much more vulnerable to material destruction due to stain localization. Particularly, as the size of grains decreases, the source of dislocations decreases and work hardening does not occur.

Studies on twin have been actively conducted as another study on microstructure deformation mechanisms related to the mechanical properties of materials. Like the grain boundaries, the twin boundary also acts as a barrier to inhibit dislocation movement and increases the stiffness of the material. At the same time, it also acts as a source of dislocations, which causes work hardening to occur in the material and helps plastic deformation[13]. Therefore, twin deformation due to material deformation has been actively progressed with the finding that the twin in the grain can bring both the rigidity and ductility of the material at the same time. However, this has not yet proceeded under extreme tensile deformation.

In this study, we first revealed the microstructure change of ultrafine grain Cu with twin embedded with extreme tensile strain behavior. We observed the microstructure of the copper thin films with TEM based EBSD (ASTAR^{TM}) according to the strain by increasing the substrate / thin film composite to 20 % after depositing the copper thin film on the polyimide substrate. Unlike the previous studies, which were not possible with extreme tensile strain due to early failure due to strain localization, the thin films deposited on a thick flexible substrate were deformed along the uniform deformation of the substrate. As a result, the thin film attached to the substrate showed tensile strain and

deformation mechanism that conventional materials could not show. It is found the microstructure of the copper thin film showed a change that was not seen before, due to the twin present in the grain. the size of the grain increased at the beginning according to the extreme tensile strain, and then gradually decreased. Our results suggest that not only the new microstructure deformation mechanism under extreme tensile deformation but also the strain delocalization and work hardening can be applied to the microstructure therefore it is believed that it can make a great contribution to research to improve the ductility of materials.

5.2. Experiment

Copper thin film was deposited onto polyimide substrate by thermal evaporation and electron beam irradiation was conducted in scanning electron microscopy. The deposition conditions and irradiation conditions described in Sec. 3.1.

In case of in-situ synchrotron XRD, the condition of Cu thin film irradiation is same, and the orientation which is used to interpret lattice strain is (111) because due to small size of Cu, not only thickness but also pad size, it was hard to get the distinguishable spectrum from other crystallographic orientations.

5.3. Texture analysis result of copper thin film during tensile deformation

Cu thin films were deposited on 125 μm polyimide substrates (Kapton HN, Dupont,

Circleville, OH) with the thickness of 100 nm. Electron beam was irradiated on Cu thin films by scanning electron microscopy (Inspect F, FEI) prior to tensile testing. (acceleration voltage: 25 kV, probe current: 10 nA, irradiation time: 10 min) then Cu thin films had a tensile strain up to 6 %, 10 %, and 20 %, respectively. (strain rate: 0.05-1). With the improvement of adhesion between Cu and PI by electron beam irradiation, Cu had almost no cracks on the surface even it was deformed with 20 % tensile strain. After stretching, abrasive milling as followed by argon ion-milling was used to reduce the thickness of PI for plan-view samples. High-voltage transmission orientation mapping in STEM was performed in an FEI Tecnai™ F20 S/TEM equipped with ASTAR™ unit. Accelerating voltage, aperture size for the nano-beam diffraction mode, and beam precession were 200 kV, 30 μm, and 1°, respectively.

Shown in Figure 5.1(a)-5.1(i) are the microstructure of Cu varying tensile strain. Figure 5.1(a)-5.1(d) are invert pole figure maps of Cu after deformed up to 0%, 6%, 10%, 20%, respectively, and Figure 5.1(e)-5.1(i) are the combination of misorientation and image quality maps of them, respectively. Interestingly, as shown in figure 1a, the texture of as-deposited Cu thin film was totally random texture, and there was no development of preferred texture during tensile deformation(Figure 5.1(b)-5.1(d)). It is also interesting that nanotwin was formed in most of the grains by simple thermal evaporation. Most of the twin planes were vertical to the in-plane direction, and some twin planes which were lied parallel or inclined to the in-plane direction were also observed in ASTAR™ of cross-sectional area..

It is important to note that, as can be seen in Figure 5.1(a)-1(i), the size of Cu grain varies with the tensile strain. Comparing Figure 5.1(a)(5.1(f)) with figure 5.1(c)(5.1(h)), there are some coalesced grains replacing uniform 100 nm sized grain when Cu was stretched to 10 %. In adittion, comparing Figure 5.1(c)(5.1(h)) with Figure 5.1(d)(5.1(i)),

coalesced grains turned into a lot of small grains when Cu was stretched further to 20 %. This change in grain size can be seen more clearly in Figure 5.1(j), which graphically shows the change of grain size with the strain. The grain size of as-deposited Cu was 93 nm, and the grain size increased from 134 nm to 147 nm while the strain increased from 6 % to 10 % and then decreased to 53 nm when the strain reached to 20 %. That is, as the tensile strain is applied, the coarsening and refinement of Cu grain occurred sequentially.

The grain coarsening and grain refinement can be more clearly confirmed by the change in misorentation during deformation. Figure 5.1(k) contains the length per unit area of misorientation with respect to tensile strain. For the analysis of misorientation, we categorized the misorientation into three boundaries: low energy boundary (misorientation < 15°), high energy boundary (misorientation > 15° and < 60°) and twin boundary (misorientation = 60°, as known as $\sum 3$ boundary). First, the length of high energy boundary decreased at 6% strain where grain coarsening occurred and increased at 20% strain where grain refinement occurred. This is due to the change in the number of grains per unit area due to grain growth and refinement, which is intuitively shown as grain growth and refinement. What is unique is that at a strain of 10%, where the size of the grain is still large, the length of the high energy boundary dramatically increases similar to that of grain refinement. It can be understood from the change in the length of the low energy boundary. The dislocations generated by the deformation are progressively turned to the low energy boundary, therefore the length of the low energy boundary increases as the strain increases. When the dislocation piles up in the low energy boundary due to continuous tensile deformation, the low energy boundary is converted to high energy boundary by the increase of misorientation due to the internal stress, and the result of 10% is thought to be caused by the conversion of low energy

boundary to the high energy grain boundary. This is supported by the rapid decrease in low energy boundary at 10%. An interesting fact of the misorientation analysis is that the length of the twin continues to change as deformation occurs. The length of the twin decreases slightly when the initial grain coalesce occurs and then increases again at 20% after grain refinement occurs. This suggests that the twin is exhausted or generated as the grain coalesce and grain refinement occur, and the twin is closely related to grain coalesce and refinement

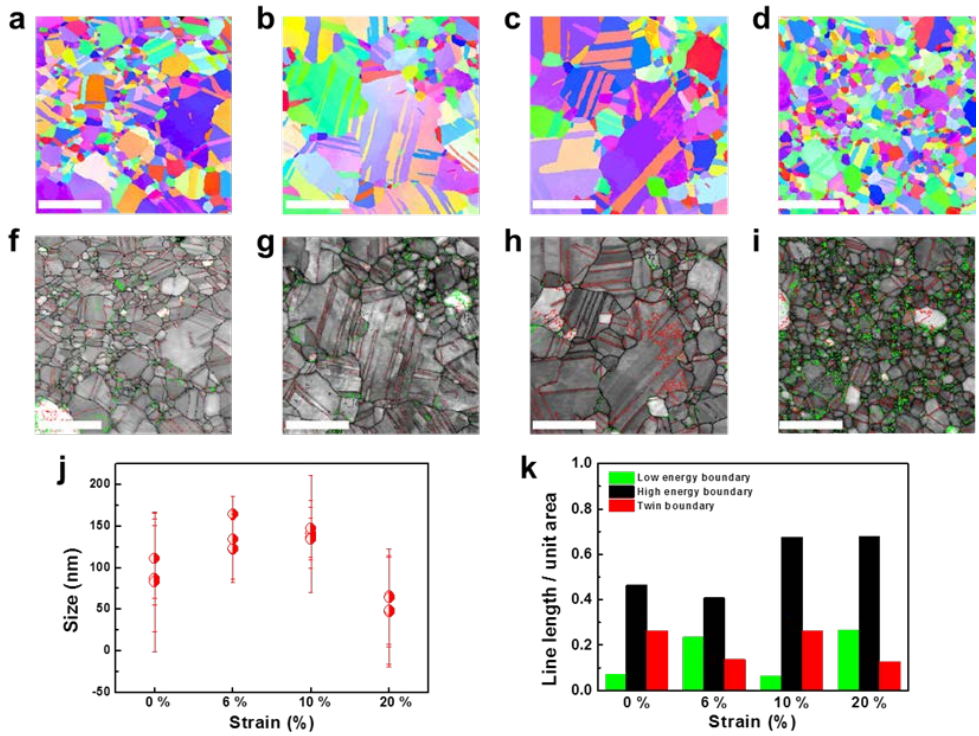

Figure 5.1 ASTAR™ results of Cu thin films on Polyimide substrate before and after tensile deformation. Invert pole figures of (a) 0 % strain, (b) 6 % strain, (c) 10 % strain and (d) 20 % strain and image quality map with misorientation of (f) 0% strain, (g) 6 % strain, (h) 10 % strain and (i) 20 % strain, respectively. (j) Average grain size and (k) distribution of misorientation varying tensile strain Scale bars, 300 nm (a-i)

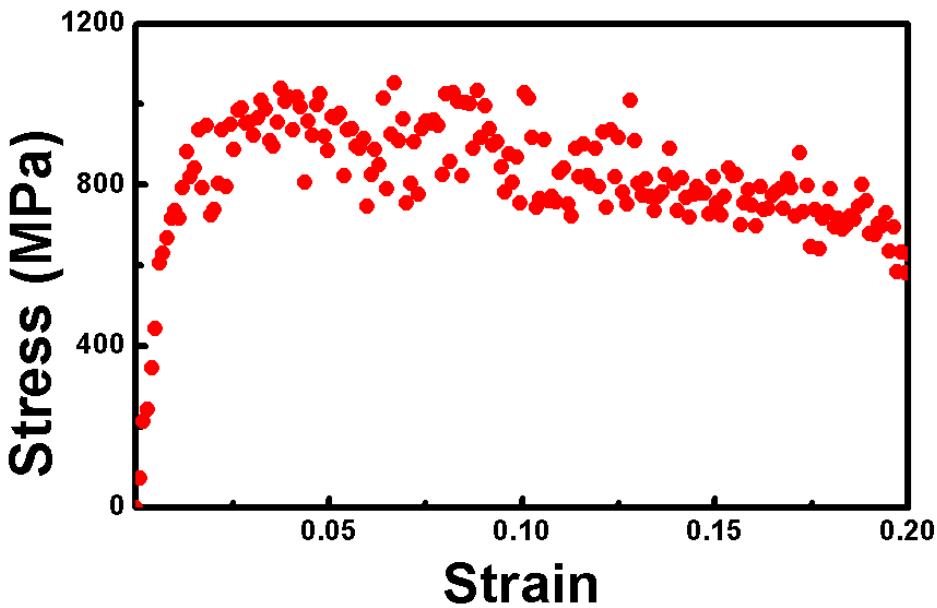

Figure 5.2 Stress-strain curve of Cu thin film measured from in-situ synchrotron XRD. Stress is calculated from lattice strain.

5.4. Deformation behavior of Cu thin film

5.4.1. Grain coarsening due to twin-grain boundary interaction

Through microstructure and stress analysis of Cu thin film, we will unveil how twin affects on grain growth and grain refinement of 100 nm sized grain, which is represented as grain boundary dissipation and subgrain formation. Figure 5.3(a) is an enlargement of grains where the grain coalesce occurs at a strain of 6%. Unlike the other grains, the grains in Figure 5.3(a) are shaped like two grains combined. It should be noted not only the shape of the grain but also the twin existing inside the grain. It seems twinning / detwinning is taking place in the grain by looking at the length and shape of the twin. Figure 5.3(b)-3(e) is a schematic diagram that simulates the process by which two grains are coalesced into a single grain based on the shape of the grain and twin found through ASTAR™. As shown in Figure 2b, when a tensile strain is applied to grain 1 (G1) and grain 2 (G2), which have twin in the inside, the twin is propagated over the grain boundary as shown in Figure 5.3(c) due to the movement of the twinning partial and its interaction with grain boundary.ref Through this process, the finely divided grain boundaries gradually disappear during the deformation due to instability (Figure 5.3(d)). Finally the two grains are coarsened in one grain by the combination of twin propagation and grain rotation due to continuous tensile deformation (Figure 5.3(e)). In order to verify the validity of this analogy, we confirmed that the stress on the copper foil at 6% strain is sufficient to cause twin partial migration. First, shear stress values for moving the leading part of twin are as follows[104, 105]

$$\tau_{twin} = \frac{Ga(4-\nu)}{8\sqrt{6}\pi(1-\nu)d\cos(\alpha-30^{\circ})}\ln\frac{\sqrt{2}d}{a}$$

Where G is the shear modulus, v is the poisson's ratio, α is the angle at which the stress is applied, d is the grain size, and a is the lattice parameter. The average grain size of the as-deposited Cu film is 93 nm, and the shear stress value calculated by the formula is about 160 MPa. On the other hand, the film stress value at 6% obtained by sXRD is about 180 MPa, which means that enough stress is applied to move the twin partials in the grain. Therefore, it can be concluded that at the initial tensile strain the grain coarsening occurred due to the movement of twining partial followed by the dissipation of grain boundary.

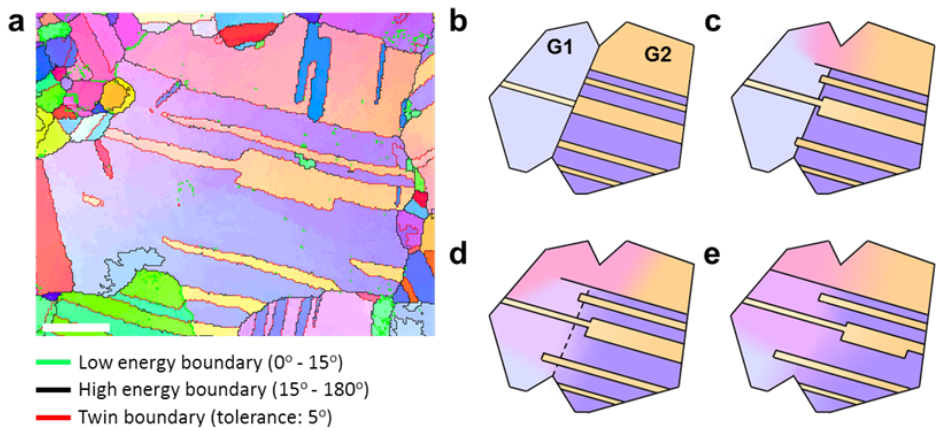

Figure 5.3 Twin-assisted grain coarsening at early stage of deformation. (a) Combination of invert pole figure and misorientation of Cu after 6 % strain. (b)-(e) schematic of twin-assisted grain coarsening. Scale bars, 100 nm,

5.4.2. Grain refinement due to twin-dislocation interaction

Interestingly, Twin is involved not only in the growth of grains, but also in the refinement of grains that occur as a result of continuous deformation. Figure 5.4 is an enlarged view of the ASTAR™ results of the Cu thin films deformed up to 10% tensile strain. In Figures 5.4(a) and 5.4(b), a white circle shows subgrain inside the grain. That is, grain refinement occurs when additional subgrain is generated inside the grains. It is worth noting that the subgrain is generated between twin boundaries (Figure 5.4(a)) or near the twin boundary (Figure 5.4(b)). Generally, dislocation cells made of dislocations existing in crystal grains are transformed into subgrain, which is a typical mechanism of subgrain generation inside grains by tensile strain. However, in the case of small grains such as 100 nm, dislocation cells and subgrain could not be produced because the dislocation density inside the grain is insufficient to form a dislocation cell due to lack of the dislocation source. Nevertheless, as shown in our ASTAR™ results, subgrain could be generated in 100 nm grains if there is twin inside of the grains. When tensile strain is applied, Twin not only acts as a dislocation source to generate the dislocation necessary to form the subgrain inside the grain, but also acts as a frame to generate the subgrain itself. This can be seen in more detail in Figures 5.4(c) and 5.4(d). Figure 5.4(c) and 5.4(d) show that the dislocations generated at the twin boundary, or the dislocations created by the disintegration of the twin boundary, are amplified and entangled and grown to a high energy boundary with a misorientation of 15 degrees or more. This is consistent with the misorientation change described in figure 1k. Since the dislocations generated in the early stage of deformation forming the low energy boundary were transformed into the high energy boundary while the deformation progressed and the misorientation increased, the length of the low energy boundary was reduced and the

length of high energy boundary was increased while maintaining the grain size at 10 % strain.

To verify if a dislocation could be created in twin, we calculated the possibility of creating a dislocation in the twin based on the sXRD result. The mechanism of generating dislocation in the twin is a soft mode in which the twin plane and the slip plane of the dislocation are parallel, and a hard mode in which the twin plane and the slip plane of the dislocation are perpendicular to each other. In soft mode, a dislocation is generated in the grain boundary near twin, and in hard mode, a dislocation is generated in a step in the twin boundary. Both mechanisms are dependent on the thickness of the twin lamella. In copper, it is known that the soft mode is dominant when the thickness of the twin lamella is less than 18 nm, and the hard mode is dominant when it is greater than 18 nm.ref In our experimental condition, the average thickness of the twin lamella over the entire range of strain is greater than 21 nm, especially since the twin lamella thickness at 6% after coarsening is 28 nm, dislocations are generated through hard mode.[106] To generate dislocations, a local stress of about 1.6 GPa is required in the twin step according to N. Lu (2015) ref. The stress value applied on the Cu thin film at 6% is 630 MPa measured by sXRD, and the local stress at the twin step obtained by multiplying the stress factor is 1.5 GPa which is quite similar to the reference. Therefore, it seems reasonable that the dislocation generated from twin through hard mode causes grain refinement by forming subgrain inside grain.

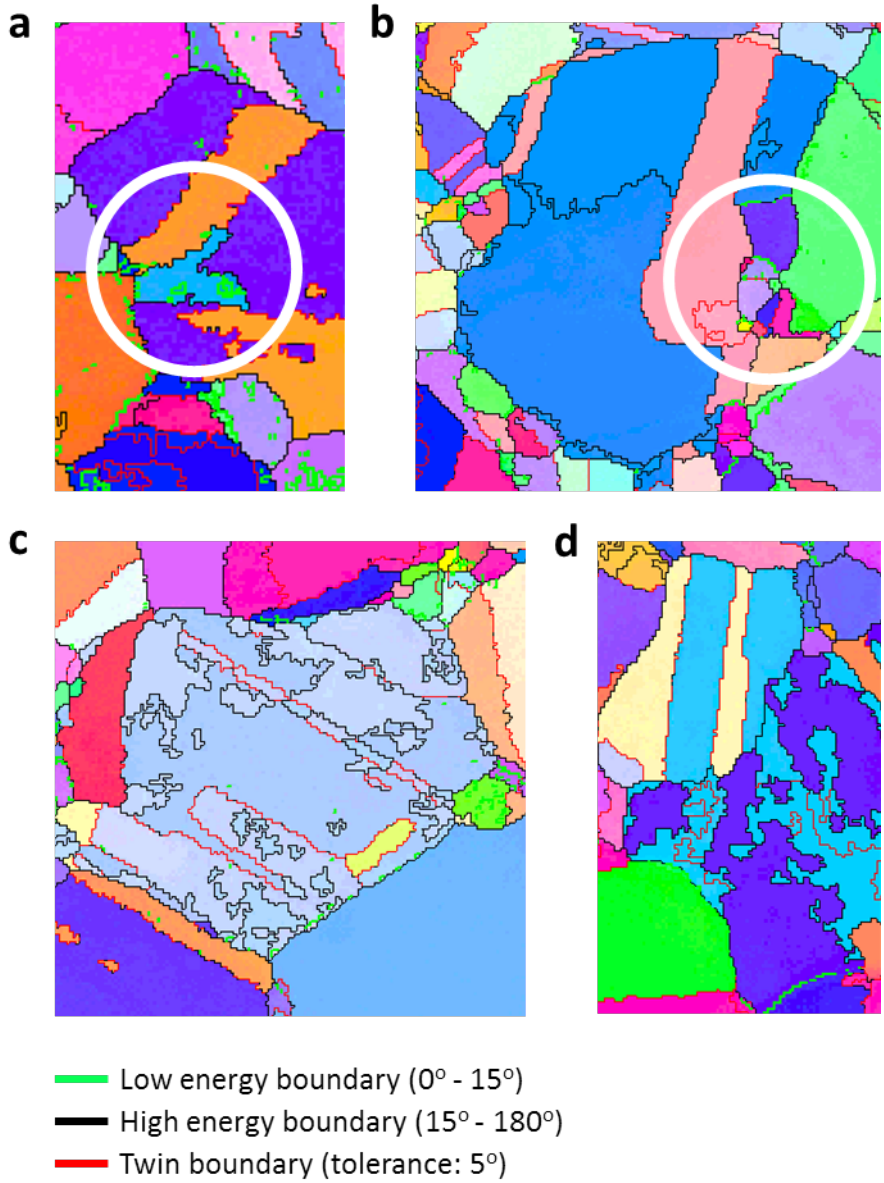

Figure 5.4 Intermediate state of grain refinement. (a), (b) Formation of subgrain near twin boundary. (c), (d) High density of high energy boundary in grain.

5.4.3. Verification by molecular dynamic simulation

In addition to the experimental results, we have further traced the twin-media ted process of grain coarsening and refinement through MD simulation. The M D simulation was carried out in two systems, Cu with (110) texture and Cu wi th random texture. The grain size and twin lamella thickness were designed to have similar values to the experimental data. Firstly, in (110) textured Cu, the progress of grain coarsening due to the dissipation of grain boundaries through the twin propagation at the initial tensile strain is shown in Fig 5.5. Figure 5.5 (a) shows grain 1 (G1) and grain 2 (G2) above and below the grain boundarie s marked by the yellow arrows along the tensile strain. As the tensile strain w as applied, the twin inside G1 and G2 propagates and meets the grain boundari es between the two grains (Figure 5.5(b)), and the twin partial breaks the grain boundaries by passing through the grain boundary (Figure 5.5(c)). The segmen ts of grain boundaries gradually disappear as the deformation progresses, and fi nally both grains are combined into one as shown in Figure 5.5(d). This twin-mediated grain coarsening also occurs in random textured Cu. Figure 5.6(a) sho ws a random texture Cu matrix and figure 5b shows an enlarged image of the grains 3 (G3) and 4 (G4). The changes of the grain boundaries between G3 an d G4 and the twin in each grain are as follows; as in (110) textured Cu, twin existing in each grain propagates over the grain boundary, and as a result, the grain boundary disappears and G3 and G4 are finally combined into one large grain.

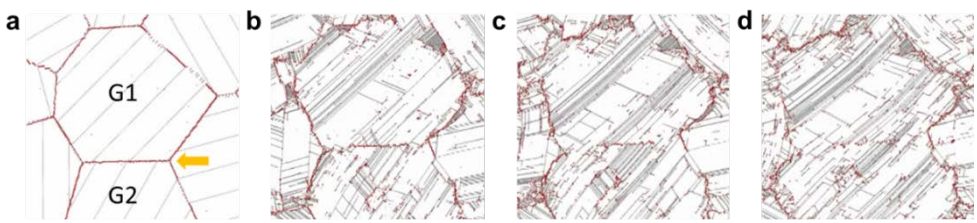

Figure 5.5 Molecular dynamic simulation result of grain coarsening in (110) oriented sample. Misorientation between two grains is 15 degree.

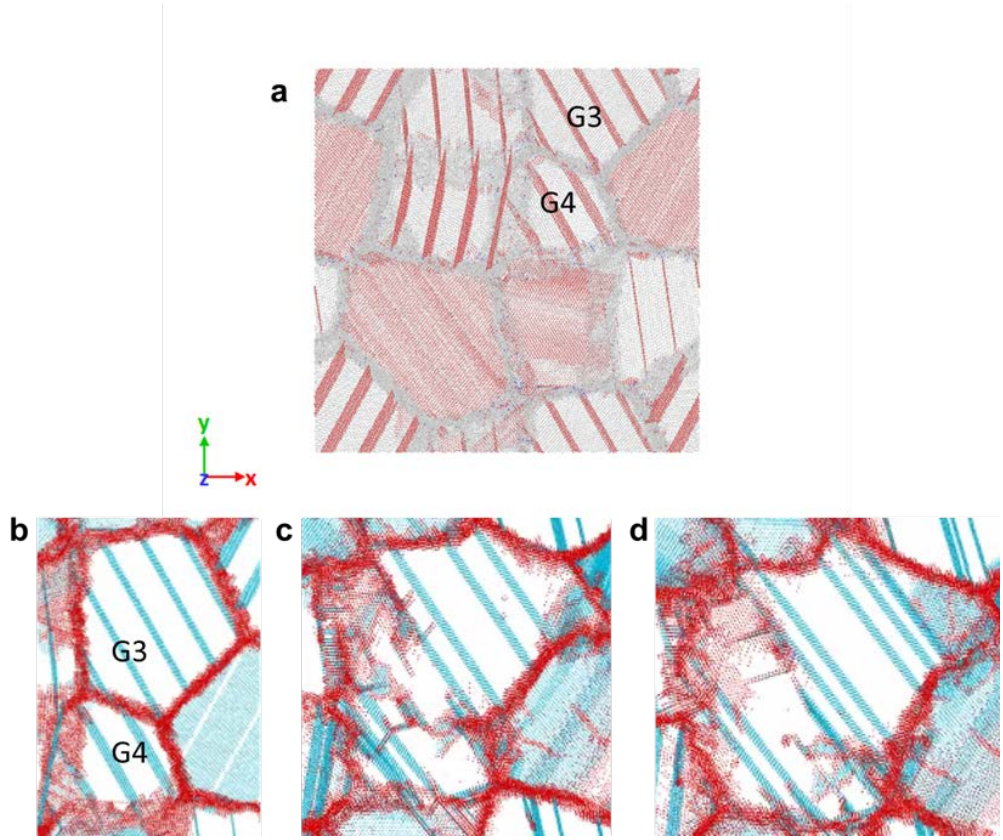

\

Figure 5.6 Molecular dynamic simulation result of grain coarsening in randomly oriented sample. Grain boundary between grain G3 and grain G4 is dissipated by propagation of twin.

Similar to grain growth, we could confirm that grain refinement is also affected by twin in the grain by MD simulation. Figure 5.7(a) shows the MD Matrix of (110) Cu undergoing the simulation. The detailed progress of grain refinement in grain 5 (G5) and grain 6 (G6) under tensile deformation are shown in Figure 5.7(b)-(d) and Figure 5.7(e)-(h), respectively. In the grain refinement process occurring in G5, as the tensile strain is applied to the crystal grains, an incline partial is formed (Figure 5.7(c)) across the twins in the grain as shown in figure 5.7(b). This incline partial is pinned while making a sessile dislocation with the existing twin boundary. The stress caused by accumulation of sessile dislocation decreases the coherency of the twin, and the dislocations within the grains are aligned to form the subgrain between the twin lamella (Figure 5.7(d)). In addition, it can be seen that grain refinement occurred in G6 accompanies grain rotation in grain refining process. The left end of the twin lamella marked by the yellow arrows at both ends of Figure 5.7(e) is slightly bent due to the stress inside the grain due to the movement and entanglement of dislocations (Figure 5.7(f)). By such continuous grain rotation, the subgrain cells consisting of twin lamella and dislocations (Figure 5.7(g)) were finally formed into subgrain with a 22 ° difference from the original position (Figure 5.7(h)). In this way, it can be confirmed that grain refinement occurs as the grains are divided into several small subgrain by incline partial generated in the twin boundary and grain rotation, which is the same as that predicted from the results of ASTAR and sXRD.

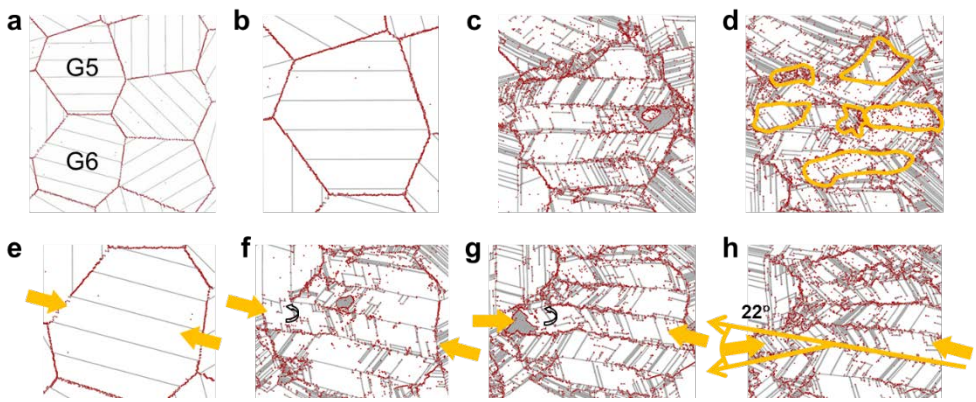

Figure 5.7 Molecular dynamic simulation result of grain refinement in (110) oriented sample by subgrain formation. (a) Total view of simulated grains and (b)-(h) are magnification fo grain G5. Grain refinement is accompanied with grain rotation (g and h)

5.5. Behavior of intergranular crack on Cu thin film

For the past decade with the emerging era of flexible devices, significant amount of investigation have been performed to understand the fracture and deformation behavior of metallic thin films on polymeric substrates under tensile deformation since this issue is directly associated with the reliability of flexible devices. However, statistically meaningful microstructural information such as texture, grain boundary characteristics and grain size have never been available particularly for nano-thin films (thickness ~100 nm) due to limitation of conventional microstructural analysis (EBSD and TEM). The lack of detailed understanding of affecting parameters in recent characterization methods such as Transmission Kikuchi Diffraction (TKD) and orientation imaging in TEM (ASTAR^{TM}) as well as difficult sample preparation have also added to the difficulty of microstructural analysis. Therefore, deformation mechanisms and fracture behavior of metallic nano-thin films on polymeric substrates have been mostly explained by continuum-based descriptions with microstructural assumptions without strong microstructural evidence.

Figure 5.8 shows a representative image quality map with inverse pole figure map of 100 nm copper thin film on polyimide substrate after tensile deformation with 20% strain. Two distinct cracks denoted as C1 and C2 are observed in the copper film and marked by white boxes. Nano-grains located along both sides of C1 and C2 cracks are marked by yellow and red lines. Using an image processing software (Adobe Photoshop), we could close the crack openings at C1 and C2 cracks by zipping the adjoining nano-grains near cracked areas as shown in Figure 5.8(b) and 5.8(c) The yellow and red crack lines overlap very well and the grain boundaries of nano-grains along both sides of the cracks match well with each other. This observation clearly

indicates that the cracks propagated along the grain boundaries. Our results support the previous study by Nan-Shu et al. which argued that the failure mode changes from transgranular cracks to intergranular cracks when the thickness of copper thin film is less than 200 nm based on the irregular notch paths from SEM observations

We further investigated the nature of grain boundaries along grains which the cracks propagated. Line misorientation measurements were extracted across five different nano-grains along C1 and C2 cracks respectively (denoted by C11 ~ C15 and C21 ~ C25), and results are listed in Table 5.1. It appears that all grains across cracks have random misorientations when the results in Table 5.1 are compared to known misorientations coherent site lattice boundaries (CSL) summarized in Table 5.2. This means that C1 and C2 cracks propagated along high energy random boundaries although there are some fine nano-grains with Σ 3 and Σ 7 boundaries near crack edges.

It is worth noting that C1 and C2 cracks stopped at triple junctions T1 and T2, respectively. As shown in Figure 5.8(d), C1 and C2 crack tips are blunt at T1 and T2 where Σ 3 and Σ 7 boundaries are present. In other words, C1 and C2 cracks could not connect by propagating through coherent grain boundaries between T1 and T2 at high tensile strain of 20%. It is speculated that crack stopping is due to lower energy of coherent boundaries. These results imply that the low- Σ coherent boundaries in nano-crystalline metallic thin films could effectively improve the resistance of crack propagation[107, 108]. However, it should be noted that our supporting information is considered as preliminary results because unraveling the fracture mechanism of copper nano-thin films requires significant amount of further systematic tests and analysis.

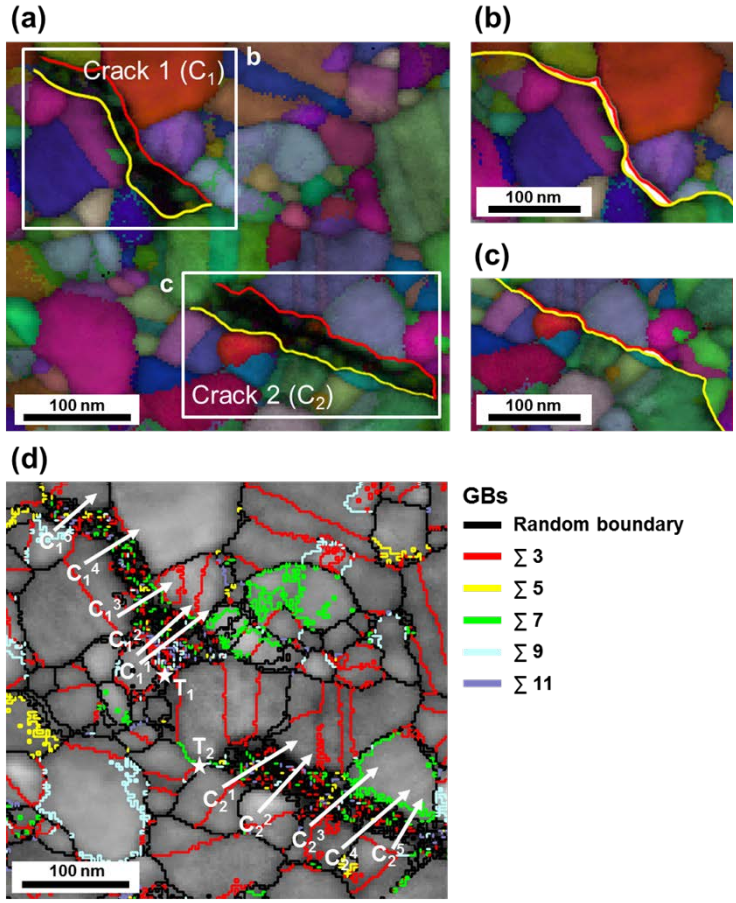

Figure 5.8 (a) Combined image quality and inverse pole figure map of 100 nm copper film on PI after 20% strain. (b) Cropped and combined image of area adjacent to crack 1. (c) Cropped and combined image of area adjacent to crack 2. (d) Combined image quality and grain boundary map of the same area as (a). Misorientations were measured between grains across both cracks C1 and C2 along white arrows. T1 and T2 are triple junctions with Σ3, Σ 7 and random boundaries

.

	Misorientation between two grains (degree)		Misorientation between two grains (degree)
C_1^1	12.9	C_2^1	50.9
C_1^2	56.3	C_2^2	42.5
C_1^3	48.3	C_2^3	44.7
C_1^4	29.5	C_2^4	25.9
C_1^5	47.7	C_2^5	34.1

Table 5.1 Misorientation between grains across cracks

∑	Misorientation angle (degree)
3	60.0
5	36.9
7	38.2
9	38.9
11	50.5

Table 5.2 Misorientation angle of coherent site lattice boundaries (CSL)

5.6. Summary

In this chapter, deformation mechanism of Cu thin film on polyimide substrate after enhancing adhesion by electron beam irradiation was investigated. Because it is believed that Cu thin film is very brittle therefore crack is nucleated only after few percent of strain, the phenomenon that Cu thin film was elongated without cracking after irradiation is unusual. Based on microstructural analysis through ASTAR™, it was revealed that Cu thin film could bear a large tensile strain without cracking because twin boundary inside of the grain continuously changed the microstructure of Cu. At the early stage of deformation, twin propagated to the neighbor grain therefore cut the grain boundaries in small ligaments. With the grain rotation, two grains were finally merged into one grain. After grain coarsening, dislocation was generated from twin step and moved from the one twin boundary to another twin boundary following its own slip plane. This twin-dislocation interaction is known as hard mode 1. Through this interaction, subgrains could be nucleated composed of twin boundaries and dislocations, and finally grain refinement was occurred. The sequentiall grain coarsening-grain refinement process due to twin boundary speculated to the plastic deformation of Cu thin film when the strain localization was prohibited by constraint substrate. Therefore it is believed that if metal has a lot of twin inside, then it has the possibility to undergo the plastic deformation, in other words, possibility to be ductile.

CHAPTER 6

Conclusion

6.1. Intrinsic and systematic factors for ductility of Cu thin film

This study investigated the realization and mechanism of large deformation of Cu thin film on polymer substrate. Contrary to common belief that thin metal is intrinsically brittle therefore it could not bear a large tensile strain, Cu thin film with 100 nm thickness in this work could be elongated without crack up to 30 % strain after electron beam irradiation. It was found that electron beam enhanced adhesion between Cu thin film and polymer substrate by increasing the interface area due to roughening by further polymerization caused by electron beam, Therefore it could be inferred that improving adhesion between two materials systematically is the one direction to fabricate reliable metal electrode and interconnects.

However, systematic factor is not the only one. Intrinsic factors driven from mechanical properties of Cu which is strongly related to the microstructure of Cu also must be considered. By the investigation of the deformation mechanism of Cu thin film through ASTAR^{TM}, it is revealed that twin boundary inside of Cu drove continuous

plastic deformation of Cu by inducing grain coarsening and grain refinement due to interaction between grain boundary and dislocation, respectively and schematic of deformation mechanism of Cu thin film is described in Figure 6.1.

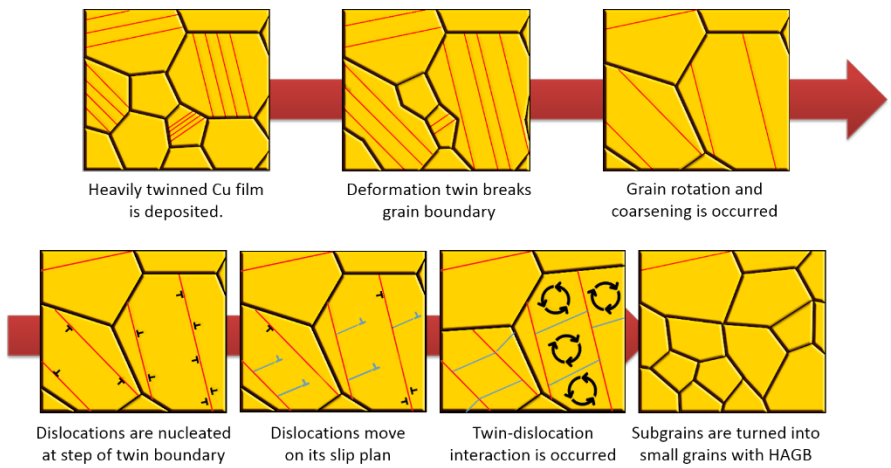

Figure 6.1 Description of the deformation behavior of Cu thin film under large deformation based on microstructural study.

6.2. Material design for the improvement of devices

Based on the insight obtained, it can be inferred that if the strain delocalization and work hardening are sufficiently applied to the material, even small sized materials could undergoes plastic deformation.

The wat to solve the strain localization is using stiff substrate as previously mentioned in section 2.2.2. However, the larger the stiffness, the harder it is to pull the substrate. Therefore if stiffness control reaches a certain level of stabilization, it is efficient to change the basic properties of metal. i.e. implant twin boundary inside of the materials.

Because tendency for nucleation of twin is closely related to stacking fault energy, it is regarded that decreasing the stacking fault energy of material by alloying could be recommended for fabricating reliable metal thin film. Also, change the deposition method which could easily induce twin could be recommended such as electroplating or DC/RF sputtering either

This thesis establishes guidelines for improving flexible devices based on the both systematic consideration and deformation behavior of metal electrode and interconnects.

6.3. Future work and suggested research

In this study, the concepts described above are based on *twin boundary*. To establish the relationship between the twin boundary and deformation mechanism, doing microstructural analysis of metals with high stacking fault energy such as aluminum or platinum which have fewer twins compared to Cu could be a good control group.

References

1. G. W. Nieman, J. R. Weertman, R. W. Siegel, *Journal of Materials Research*, **6** (1991)
2. R. Z. Valiev, E. V. Kozlov, Yu. F. Ivanov, J. Lian, A. A. Nazarov, B. Baudelet, *Acta Matallurgica et Materialia*, **42** (1994)
3. Y. M. Wang, M. Chen, F. Zhou, E. Ma, *Nature*, **419**, 6910 (2002)
4. Y. Champion, C. Langlois, S. Guérin-Mailly, P. Langlois, J.-L. Bonnentien, M. J. Hÿtch, *Science*, **300** (2003)
5. Y. M. Wang, K. Wang, D. Pan, K. Lu, K. J. Hemker, E. M, *Scripta Materialia*, **48** (2003)
6. K. Maki, Y. Ito, H. Matsunaga, H. Mori, *Scripta Materialia*, **68**, 10 (2013)
7. Y. Ito, H. Matsunaga, H. Mori, K. Maki, *Material Transactions*, **55** (2014)
8. G. Shi, X. Chen, H. Jiang, Z. Wang, H. Tang, Y. Fan, *Materials Science and Engineering A*, **636** (2015)
9. O. Kraft, M. Hommel, E. Arzt, *Materials Science and Engineering A*, **288** (2000)
10. N. Lu, Z. Suo, J. Vlassak, *Acta Materialia*, **58** (2010)
11. Aaron Kobler, A. M. Hodge, H. Hahn, C. Kübel, *Applied Physics Lettters*, **106** (2015)
12. S. Kim, X. Li, H. Gao, S. Kumar, *Acta Materialia*, **60** (2012)
13. L. Lu, Y. Shen, X. Chen, L. Qian, K. Lu, *Science*, **304** (2004)
14. D. Xu, W. L. Kwan, K. Chen, X, Zhang, V. Ozoliņš, K. N. Tu, *Applied Physics Letters*, **91** (2007)

15. L. Lu, X. Chen, X. Huang, K. Lu, *Science*, **323** (2009)
16. Y. T. Zhu, X. Z. Liao, X. L. Wu, *Progress in Materials Science*, **57** (2012)
17. J. R. Greer, *Nature Materials*, **12** (2013)
18. R. Huang, J.H. Prévost, Z. Suo, *Acta Materialia*, **50** (2002)
19. T. Li, Z. Y. Huang, Z. C. Xi, S. P. Lacour, S. Wagner, Z. Suo, *Mechanics of Materials*, **37** (2005)
20. T. Li, Z. Suo, *International Journal of Solids and Structure*, **43** (2006)
21. T. Li, Z. Huang, Z. Suo, S. P. Lacour, S. Wagner, *Applied Physics Letters*, **88** (2004)
22. J. A. Fan, W.-H. Yeo, Y. Su, Y. Hattori, W. Lee, S.-Y. Jung, Y. Zhang, Z. Liu, H. Cheng, L. Falgout, M. Bajema, T. Coleman, D. Gregoire, R. J. Larsen, Y. Huang, J. A. Rogers, *Nature Communication*, **5** (2014)
23. C. F. Guo, T. Sun, Q. Liu, Z. Suo, Z. Ren, *Nature Communications*, **5** (2013)
24. K. Mirpuri, H. Wendrock, S. Menzel, K. Wetzig, and J. Szpunar, *Thin Solid Films*, **496** (2006)
25. J. H. Han, K. H. Oh, J. C. Lee, *Materials Science and Engineering A*, **240** (2004)
26. R. E. Reed-Hill, *Physical Metallurgy Principles*, D. Van Nostrand Company, New Work, USA
27. M.. A. Meyers, K. K. Chawla, *Mechanical behavior of Materials*, Cambridge University Press, New York, USA
28. D. Maharaj, B. Bhushan, *Beilstein Journal of Nanotechnology*, **5** (2014)
29. T. J. Massart, T. Pardoen, *Acta Materialia*, **58** (2010)
30. C. Y. Yu, P. W. Kao, C. P. Chang, *Acta Materialia*, **53** (2005)

31. P. Bhaskar, A. Dasgupta, V.S. Sarma, U.K. Mudali, S. Saroja, *Materials Science and Engineering A*, **616** (2014)
32. Y. Ivanisenko, L. Kurmanaeva, J. Weissmueller, K. Yang, J. Markmann, H. Rosner, T. Scherer, H.J. Fecht, *Acta Materialia*, **57** (2009)
33. P. Liu, S. Mao, L. Wang, X. Han, Z. Zhang, *Scripta Materialia*, **64** (2011)
34. T. Rupert, D. Gianola, Y. Gan, K. Hemker, *Science*, **326** (2009)
35. K. Zhang, J.R. Weertman, J.A. Eastman, *Applied Physics Letters*, **87** (2005)
36. D.S. Gianola, S. Van Petegem, M. Legros, S. Brandstetter, H. Van Swygenhoven, K.J. Hemker, *Acta Materialia*, **54** (2006)
37. M. Legros, D.S. Gianola, K.J. Hemker, Acta Materialia, **56** (2008)
38. T. Gorkaya, D.A. Molodov, G. Gottstein, Acta Materialia, **57** (2009)
39. F. Mompiou, D. Caillard, M. Legros, Acta Materialia, **57** (2009)
40. Q. Yu, M. Legros, A. M. Minor, *MRS Bulletin*, **40** (2015)
41. J.W. Christian, S. Mahajan, *Progress in Materials Science*, **39** (1995)
42. X.L. Wu, X.Z. Liao, S.G. Srinivasan, F. Zhou, E.J. Lavernia, R.Z. Valiev, *Physical Review Letters*, **100** (2008)
43. T.H. Blewitt, R.R. Coltman, J.K. Redman, *Journal of Applied Physics*, **28** (1957)
44. M.A. Meyers, U.R. Andrade, A.H. Choksh, *Metallurgical and Materials Transactions A*, **26** (1995)
45. M.A. Meyers, F. Gregori, B.K. Kad, M.S. Schneider, D.H. Kalantar, B.A. Remington, *Acta Materialia*, **51** (2003)
46. L.E. Murr, Residual microstructure–mechanical property relationships in shock-loaded metals and alloys, *Plenum Press*, New York (NY) (1981)

47. F. Cao, I.J. Beyerlein, F.L. Addessio, B.H. Sencer, C.P. Trujillo, E.K. Cerreta, *Acta Materialia*, **58** (2010)
48. T. Li, Z. Suo, *International Journal of Solids and Structures*, **44** (2007)
49. B. Wang, H. Idrissi, H. Shi, M.S. Colla, S. Michotte, J.P. Raskin, T. Pardoen, D. Schryvers, *Scripta Materialia*, **66** (2012)
50. M.S. Colla, *Plasticity and creep in thin free-standing nanocrystalline Pd films* (Ph.D. dissertation), Université catholique de Louvain (2014)
51. E.W. Qin, L. Lu, N.R. Tao, J. Tan, K. Lu, *Acta Materialia*, **57** (2009)
52. B.J. Jeon, S. Lee, J.K. Lee, *Surface and Coatings Technology*, **202** (2008)
53. D.R. Clarke, W. Pompe, Acta Materialia, **47** (1999)
54. W.T.S. Huck, N. Bowden, P. Onck, T. Pardoen, J.W. Hutchinson, G.M. Whitesides, *Langmuir*, **16** (2000)
55. D.Y. Khang, H. Jiang, Y. Huang, J.A. Rogers, *Science*, **311** (2006)
56. O. Graudejus, Z. Jia, T. Li, S. Wagner, *Scripta Materialia*, **66** (2012)
57. N. Bowden, S. Brittain, A.G. Evans, J.W. Hutchinson, G.M. Whitesides, *Nature*, **393** (1998)
58. X. Zhang, A. Misra, *Scripta Materialia*, **66** (2012)
59. W. Xu, J. S. Yang, T. J. Lu, *Maters & Design*, **32** (2011)
60. K. Lu, *Nature Reviews Mateirals*, **1** (2016)
61. T. Zhu, H. Gao, Scripta Materialia, **66** (2012)
62. X. M Luo, X. F. Zhu, G. P. Zhang, *Nature Communications*, **5** (2014)
63. J. Li, J. Y. Zhang, L. Jiang, P. Zhang, K. Wu., G. Liu, J. Sun, *Materials Science and Engineering A*, **628** (2015)
64. G. Wang, G. Li, L. Zhao, J. Lian, Z. Jiang, Q. Jiang, *Materials Science and Engineering A*, **527** (2010)

65. M.-S. Colla, B. Wang, H. Idrissi, D. Schryvers, J.-P. Raskin, T. Paradoen, *Acta Materialia*, **60** (2012)

66. S. I. Rao, D. M. Dimiduk, T. A. Parthasarathy, M. D. Uchic, M. Tang, C. Woodward, *Acta Materialia*, **56** (2008)

67. A. A. Benzerga, *International Journal of Plasticity*, **24** (2008)

68. A. A. Benzerga, N. F. Shaver, *Scripta Materialia*, **54** (2006)

69. T. A. Parthasarathy, S. I. Rao, D. M. Dimiduk, M. D. Uchic, D. R. Trinkle, *Scripta Materialia*, **56** (2007)

70. F. Mompiou, M. Legros, M. Coulombier, J.P. Raskin, T. Pardoen, Acta Materialia, **61** (2013)

71. H. Idrissi, A. Kobler, B. Amin-Ahmadi, M. Coulombier, M. Galceran, J.P. Raskin, S. Godet, C. Kubel, T. Pardoen, D. Schryvers, *Applied Physics Letters*, **104** (2014)

72. N. Lu, X. Wang, Z. Suo, J. Vlassak, *Applied Physics Letters*, **91** (2007)

73. Y. Arafat, I. Dutta, and R. Panat, *Applied Physics letters*, **107** (2015)

74. S.-Y. Lee, H.-U. Guim, D.-I. Kim, Y.-C. Joo, C.-H. Shim, J.-P. Ahn, I.-S. Choi, M. Abbasi, Scripta Materialia, **138** (2017)

75. M. Kim, D. Ha, T, Kim, Nature Communications, **6** (2015)

76. D. Huh, K. L. Mills, X. Zhu, M. A. Burns, M. D. Thouless, S. Takayama, *Nature Materials*, **6** (2007)

77. D. J. Green, R. Tandon, V. M. Sglavo, *Science*, **283** (1999)

78. K. H. Nam, I. H. Park, S. H. Ko, *Nature*, **485** (2012)

79. K. H. Nam, Y. D. Suh, J. Yeo, D. Woo, *Scientific Reports*, **6** (2015)

80. R. Adelung, O. C. Aktas, J. Franc, A. Biswas, R. Kunz, M. Elbahri, J. Kanzow, U. Schürmann, F. Faupe, *Nature Materials*, **3** (2004)

81. B. E. Alaca, H. Sehitoglu, T. Saif, *Applied Physics Letters*, **84** (2004)

82. D. Kang, P. V. Pikhitsa, Y. W. Choi, C. Lee, S. S. Shin, L. Piao, B. Park, K. Y. Suh, T. I. Kim, M. Choi, *Nature*, **516** (2014).

83. Y. W. Choi, D. Kang, P. V. Pikhitsa, T. Lee, S. M. Kim, G. Lee, D. Tahk, M. Choi, *Scientific Reports*, **7** (2017)

84. D. Drouin, A. R. Courture, D. Joly, X. Tastet, V. Aimez, R. Gauvin, *Scanning*, **29** (2007)

85. F. E. Komissarenko, I. S. Mukhin, A. O. Golubok, N. V. Nikonorov, M. A. Prosnikov, A. I. Sidorov, *Journal of Micro/Nanolithography, MEMS, and MOEMS*, **15** (2016)

86. V. E. Cosslett, R. N. Thomas, *British Journal of Applied Physics*, **15** (1964)

87. V. E. Cosslett, R. N. Thomas, *British Journal of Applied Physics*, **16** (1965)

88. V. E. Cosslett, R. N. Thomas, *British Journal of Applied Physics*, **15** (1964)

89. B. Voigtländer, U. Linke, H. Stollwerk, J. Brona, *Journal of Vacuum Science & Technology A: Vacuum, Surfaces, and Films*, **23** (2005)

90. D. J. T. Hill, J. L. Hopewell, *Radiation Physics and Chemistry*. **48** (1996)

91. T. Sasuga, N. Hayakawa, K. Yoshida and M. Hagiwara, *Polymer*, **26** (1985)

92. H. Tahara, T. Kawabata, L. Zhang, T. Yasui, T. Yoshikawa, *Nuclear Instruments and Methods in Physics Research B*, **121** (1997)

93. V. I. Zyn, *Radiation Physics and Chemistry*, **122** (2016)

94. P.-H. Kang, Y.-K. Jeon, J.-P. Jeun, J.-W. Shin, Y.-C. Nho, *Journal of Industrial and Engineering Chemistry*, **14** (2008)

95. N. L. Mathakari, V. N. Bhoraskar, S. D. Dhole, *Materials Science and Engineering B*, **168** (2010)

96. Hirotsugu Yasuda, Luminous Chemical Vapor Deposition and Interface Engineering, *CRC Press* (2004)

97. S.J. Bull, D.S. Rickerby, A. Matthews, A. Leyland, A.R. Pace, J. Valli, *Surface and Coatings Technology*, **36** (1988)

98. T. Sakai, A. Belyakov, R. Kaibyshev, H. Miura, J. J. Jonas, *Progress in Materials Science*, **60** (2014)

99. A. Belyakov, T. Sakai, H. Miura, K. Tsuzaki, *Philosophical Magazine A*, **81** (2001)

100. D. Hardwick, C. M. Sellars, W. J. Tagart, *Journal of the Japan Institute of Metals and Materials*, **90** (1961)

101. A. Belyakov, W. Gao, H. Miura, T. Sakai, *Metallurgical and Materials Transactions A*, **29A** (1998)

102. A. Belyakov, H. Miura, T. Sakai, *The Iron and Steel Institute of Japan International*, **38** (1998)

103. C. Kobayashi, T. Sakai, A. Belyakov, H. Miura, *Philosophical Magazine Letters*, **87** (2007)

104. Y. T. Zhu, X. Z. Liao, Y. H. Zhao, S. G. Srinivasan, F. Zhou, and E. J. Lavernia, *Applied Physics Letters*, **85** (2004)

105. Y. T. Zhu, X. Z. Liao, S. G. Srinivasan, E. J. Lavernia, *Journal of Applied Physics*, **98** (2005)

106. N. Lu, K. Du, L. Lu, H. Q. Ye, Nature Communications, **6** (2015)

107. S. Kobayashi, T. Maruyama, S. Saito, S. Tsurekawa, T. Watanabe, Journal of Materials Science, **49** (2014)

108. T. Watanabe, S. Tsurekawa, Acta Materialia. **47** (1999)

요약(국문초록)

유연 소자가 향후 전자 소자의 새로운 패러다임으로 떠오름에 따라 유연 소자의 신뢰성을 향상시키는 연구가 각광을 받고 있다. 유연 소자의 신뢰성은 소자의 전기적 특성의 근간을 이루는 금속 박막의 신뢰성과 매우 밀접하게 연관되어 있기 때문에 금속 박막의 신뢰성 향상은 곧 유연 소자의 신뢰성 향상으로 이어진다. 기존의 딱딱하고 변형하지 않는 기판 위에 증착된 금속 박막과는 달리 유연 소자 위에 증착된 금속 박막은 지속적인 기계적 변형에 노출되며, 기계적 변형에 따른 금속 박막의 파괴는 곧 전기적 성질의 저하로 이어져 소자의 파괴를 야기한다. 따라서 우수한 기계적 신뢰성을 가지는 금속 박막의 개발 및 이를 가능하게 만들어줄 변형 메커니즘의 이해는 필수적이다.

금속 박막의 빠른 파괴는 재료적 측면과 구조적 측면 모두에서 야기된다. 먼저 재료적 측면에서는 재료의 박막화에 따른 결정립 크기의 감소로 인해 결정립 내부에서 전위의 이동이 제한됨에 따라 소성 변형이 어려워진다. 뿐만 아니라 전위 생성원의 수 또한 적어 소성 변형을 위한 지속적인 변위 생성이 불가하다. 따라서 크기가 작은 결정립을 가지는 재료는 소성 변형이 발생하지 못해 탄성 변형 후 곧장 파괴를 겪는다.

한편 구조적 차원에서는, 재료 내부의 전위가 표면으로 쉽게 빠져나가 소성 변형을 저해시킬 뿐 아니라 표면의 굴곡 및 결함에 응력이 집중되면서 빠른 파괴를 야기한다. 이렇듯 박막화로 인한 표면효과의 극대화는 박막을 기판 위에 증착시켜 구조체의 두께를 증가시키는 방법으로 어느 정도 해결할 수 있다. 이 경우, 금속 박막에 비해 낮은 모듈러스와 높은 탄성 한계 변형률을 가지는 유연 기판과 함께 움직여야 하기 때문에 금속 박막의 파괴 메커니즘은 두 재료의 상이한 기계적 성질 차이에 영향을 받는다. 특히, 기계적 성질의 차이는 인장 변형

시 금속 박막의 박리를 야기하는데, 박리된 금속 박막은 기판이 존재하지 않는 상태에서의 변형을 그대로 따라가기 때문에 박리는 곧 금속 박막의 파괴를 야기한다.

따라서 기계적 신뢰성이 우수한 금속 박막을 설계하기 위해서는 먼저 박리를 억제하는 구조체의 설계가 필요하다. 금속 박막이 분리 없이 유연 기판을 따라 고르게 변형할 경우 소성 변형이 고르게 야기되어 파괴 없이 변형이 가능하다. 또한 이와 같은 구조체가 만들어 졌을 경우, 꾸준한 소성 변형이 가능하도록 구리 내부에 전위가 꾸준하게 공급되어야 한다. 즉, 내부에 전위를 계속적으로 인가해 줄 수 있는 미세구조를 설계할 수 있어야 하며, 이를 위해서는 인장 변형 시 박막의 미세구조가 어떻게 변화하는지에 대한 포괄적인 이해가 우선되어야 한다. 하지만 박막 내부에 존재하는 결정립은 통상적으로 사용되는 미세구조 분석 기구인 전자 후방산란 회절분석기 (EBSD) 의 분해능보다 작기 때문에 기존의 EBSD 로는 미세구조의 분석이 어렵다는 문제가 있다.

본 연구에서는 먼저 전자 소자에 대표적으로 사용되는 전도체인 구리 박막의 신뢰성 향상을 위한 구조적 차원에서의 설계를 전자빔 조사라는 새로운 방법을 통해 진행하였다. 구리 박막 위로 전자빔을 조사할 경우 구리 박막과 유연 기판 사이의 접착력이 향상되어 구리 박막의 박리를 억제하고, 따라서 박리에 의한 박막의 파괴가 억제되기 때문에 30 % 라는 인장 변형률 하에서도 표면에 균열이 거의 나지 않는 거동을 보일 수 있었다. 전자빔 조사의 계면 접착력 향상은 스크래치 테스트와 계장화 압입 시험을 통해 확인하였으며, 이를 통해 전자빔에 의해 변형된 유연 기판이 접착력 향상을 야기하는 것을 확인할 수 있었다. 우수한 기계적 성질은 우수한 전기적 성질과 이어진다는 특성을 근간으로 전자빔을 조사한 부분에서는 파괴가 나지 않는 인광 유기 발광 소자를 제작하여 향후 유연소자 제작 및 반응소자 제작에 필요한 패터닝 기술로 활용될 수 있는 가능성을 확인하였다.

또한 구리 박막의 기계적 변형에 따른 미세구조 변형 기작을 규명하여 보다 우수한 기계적 성질을 가지는 재료의 설계에 대한 재료적 관점에서의 안목을 제시하였다. 크기가 채 100 nm 에 불가한 결정립의 미세구조 분석을 위해 기존의 EBSD 가 아닌 투과주사현미경을 기반으로 한 미세구조 분석 기술인 ASTAR™ 를 이용하여 미세구조 분석을 진행하였으며, 그 결과 구리 박막 내부에 존재하는 높은 밀도의 쌍정 경계가 재료 내부에 걸리는 응력 및 변형 에너지를 균열이 아닌 미세구조 변화를 통해 해소할 수 있도록 도와주는 것을 확인할 수 있었다. 쌍정 경계는 결정립 사이를 전파하는 과정에서 결정립의 조대화를 야기할 뿐 아니라, 쌍정 경계에서 발생한 전위와의 상호작용을 통해 쌍정 경계-전위 구조를 만듦으로써 결정립의 미세화를 야기하였다. 이와 같은 미세구조 변화를 통해 전자빔이 조사된 구리 박막은 높은 인장 변형률 하에서도 파괴 없이 꾸준하게 소성 변형을 이어갈 수 있었다.

본 연구는 취성이 크다고 알려진 미세한 미세구조를 가지는 재료에서도 꾸준한 전위의 공급과 변형률 국소화(strain localization) 문제가 해결된다면 소성변형을 통해 향상된 연성을 가질 수 있음을 전자빔 조사를 통해 구현하고 미세구조 분석을 통해 규명한 연구이다. 이를 통해 유연 소자의 성능과 신뢰성을 향상시키기 위한 금속 박막 재료 설계에 대한 기준을 제시하였다.

표제어: 금속 재료, 기계적 거동, 유연 소자, 구리 박막, 계면 접착력, 전자빔 후처리, 미세 구조 분석.

학 번: 2011-20657